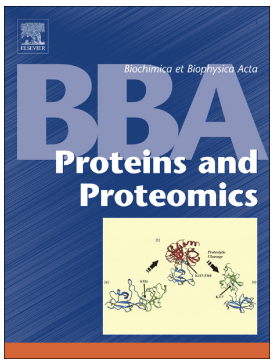

Engineering methionine γ-lyase from Citrobacter freundii for anticancer activity

Samanta Raboni, Svetlana Revtovich, Nicola Demitri, Barbara Giabbai, Paola Storici, Chiara Cocconcelli, Serena Faggiano, Elena Rosini, Loredano Pollegioni, Serena Galati, Annamaria Buschini, Elena Morozova, Vitalia Kulikova, Alexey Nikulin, Edi Gabellieri, Patrizia Cioni, Tatyana Demidkina, Andrea Mozzarelli

PII:	S1570-9639(18)30165-1
DOI:	doi:10.1016/j.bbapap.2018.09.011
Reference:	BBAPAP 40145
To appear in:	*BBA - Proteins and Proteomics*
Received date:	19 June 2018
Revised date:	27 August 2018
Accepted date:	25 September 2018

Please cite this article as: Samanta Raboni, Svetlana Revtovich, Nicola Demitri, Barbara Giabbai, Paola Storici, Chiara Cocconcelli, Serena Faggiano, Elena Rosini, Loredano Pollegioni, Serena Galati, Annamaria Buschini, Elena Morozova, Vitalia Kulikova, Alexey Nikulin, Edi Gabellieri, Patrizia Cioni, Tatyana Demidkina, Andrea Mozzarelli , Engineering methionine γ-lyase from Citrobacter freundii for anticancer activity. Bbapap (2018), doi:10.1016/j.bbapap.2018.09.011

Engineering Methionine γ-Lyase from *Citrobacter freundii* for Anticancer Activity

Samanta Raboni[a,b], Svetlana Revtovich[c], Nicola Demitri[d], Barbara Giabbai[d], Paola Storici[d], Chiara Cocconcelli[a], Serena Faggiano[a,b], Elena Rosini[e], Loredano Pollegioni[e], Serena Galati[f], Annamaria Buschini[f], Elena Morozova[c], Vitalia Kulikova[c], Alexey Nikulin[g], Edi Gabellieri[b], Patrizia Cioni[b], Tatyana Demidkina[c*] and Andrea Mozzarelli[a,b,h*]

[a]Department of Food and Drug, University of Parma, Parma, Italy

[b]Institute of Biophysics, National Research Council, Pisa, Italy

[c]Engelhardt Institute of Molecular Biology of the Russian Academy of Sciences, Moscow, Russia

[d]Elettra Synchrotron Trieste, Trieste, Italy

[e]Department of Biotechnology and Life Sciences – University of Insubria, Varese, Italy

[f]Department of Chemistry, Life Sciences and Environmental Sustainability, University of Parma, Parma, Italy

[g]Institute of Protein Research, Russian Academy of Sciences, Pushchino, Russia

[h]National Institute of Biostructures and Biosystems, Rome, Italy

*Corresponding Authors:

Andrea Mozzarelli, Department of Food and Drug, University of Parma, Parma, Italy. Email: andrea.mozzarelli@unipr.it

Tatyana Demidkina, Engelhardt Institute of Molecular Biology of the Russian Academy of Sciences, Moscow, Russia. Email: tvd@eimb.ru

RUNNING TITLE: Methionine γ-lyase engineering

ABBREVIATIONS:

MGL, methionine γ-lyase; PLP, pyridoxal 5'-phosphate; HO-Hxo-DH, D-2-hydroxyisocaproate dehydrogenase; DNPH, 2,4-dinitrophenylhydrazine; NADH, nicotinamide adenine dinucleotide reduced form; DTT, D,L-dithiothreitol; LB, Luria–Bertani; MMEPEG, polyethylene glycol monomethyl ether; DMEM, Dulbecco's Modified Eagle Medium; FBS, fetal bovine serum.

HIGHLIGHTS

- The C-terminal loop of *C. freundii* MGL is highly variant
- Most mutations at positions P357, V358, P360 and A366 cause enzyme inactivation
- Variant V358Y showed two-fold increase in catalytic rate and K_M.
- Comparison of X-ray structures of MGLs and V358Y suggests a conformational adaptation to mutations

KEYWORDS: Site-saturation mutagenesis; pyridoxal 5'-phosphate dependent enzyme; protein engineering; methionine depletion; cytotoxicity activity; cancer therapy.

ABSTRACT

Methionine deprivation of cancer cells, which are deficient in methionine biosynthesis, has been envisioned as a therapeutic strategy to reduce cancer cell viability. Methionine γ-lyase (MGL), an enzyme that degrades methionine, has been exploited to selectively remove the amino acid from cancer cell environment. In order to increase MGL catalytic activity, we performed sequence and structure conservation analysis of MGLs from various microorganisms. Whereas most of the residues in the active site and at the dimer interface were found to be conserved, residues located in the C-terminal flexible loop, forming a wall of the active site entry channel were found to be variable. Therefore, we carried out site-saturation mutagenesis at four independent positions of the C-terminal flexible loop, P357, V358, P360 and A366 of MGL from *Citrobacter freundii*, generating libraries that were screened for activity. Among the active variants, V358Y exhibits a 1.9-fold increase in the catalytic rate and a 3-fold increase in K_M, resulting in a catalytic efficiency similar to wild type MGL. V358Y cytotoxic activity was assessed towards a panel of cancer and nonmalignant cell lines and found to exhibit IC_{50} lower than the wild type. The comparison of the 3D-structure of V358Y MGL with other MGL available structures indicates that the C-terminal loop is either in an open or closed conformation that does not depend on the amino acid at position 358. Nevertheless, mutations at this position allosterically affects catalysis.

1. INTRODUCTION

A striking metabolic difference between normal and many human tumor cells is the dependence of cancer cells on L-methionine, an essential amino acid, for survival and proliferation. Normal cells do not suffer from methionine deficiency since they possess the ability to grow on homocysteine, one of methionine metabolic precursor. The high frequency of methionine auxotrophy in cancer cells suggested that it might be a general metabolic feature of cancer cells, termed "Hoffman effect" [1], and an important aspect of oncogenic transformation, analogous to the "Warburg effect" for glucose. Consequently, methionine depletion has gained increased recognition as a tumor specific therapeutic strategy. This, in turn, has led to the exploitation of methionine-restricted diet and methionine-degrading enzymes for the depletion of plasma methionine to limit cancer cells proliferation [2, 3]. The most frequently used enzyme is methionine γ-lyase (EC 4.4.1.11, MGL), which degrades L-methionine to α-ketobutyrate, ammonia and methanethiol via a α,γ-elimination reaction [4]. Several strategies have been adopted to deliver MGL to cancer cells. These include free and polyethylene glycol-conjugated MGL [5-8], erythrocytes loaded with MGL [9], stealth PLGA/liposome-containing MGL [10] and gene therapy based on adenoviral vector carrying the MGL gene [11]. Recent studies proved the efficacy of MGL in a patient-derived orthotopic xenograft model, suggesting potential clinical development, especially in recalcitrant cancers such as Ewing's sarcoma [12-17].

MGL is assigned to the aspartate aminotransferase family of pyridoxal 5'-phosphate (PLP)-dependent enzymes and exhibits the structural features characteristic of a fold type I [18-21]. The three-dimensional structure of wild type MGL in the absence and presence of substrate analogues has been determined [22-29]. MGL is a tetrameric enzyme composed of four identical subunits with two tightly associated dimers forming the active site at the dimer interface. Each subunit consists of an N-terminal domain, the PLP-binding domain and the C-terminal domain. PLP is located within a

rather deep cavity on the dimer surface bound via a Schiff base to K210 (*C. freundii* numbering) [23, 24, 27, 30].

Considering the therapeutic potential of MGL as an anticancer agent, our goal was to engineer the enzyme from *C. freundii* to improve its catalytic activity by using semi-rational design, known as site-saturation mutagenesis [31-34]. The integration of structural information and evolution analysis of MGL guided the selection of candidate residues to be replaced. A parallel effort is aimed at the development of suitable MGL formulation for *in vivo* delivery [35].

2. MATERIALS AND METHODS

2.1. *Materials* - L-Methionine, D,L-homocysteine, S-methyl-L-cysteine, cysteine, nicotinamide adenine dinucleotide reduced form (NADH), PLP, ampicillin, Luria-Bertani broth, tryptone, and yeast extract were purchased from Sigma-Aldrich (San Louis, MO). D,L-dithiothreitol (DTT) was from Applichem (Darmstadt, Germany). DEAE-sepharose was from GE Healthcare Life Sciences (Pittsburg, PA, USA). The plasmid with the gene of HO-Hxo-DH was a kind gift of K. Muratore (University of California, Berkeley, Department of Molecular and Cell Biology, Berkeley, CA, USA). The *E. coli* strain BL21 (DE3) *F- ompT hsdSB gal dcm* (DE3) (Merck, Darmstadt, Germania) was used to express *C. freundii* MGL and the mutants.

2.2. *Structure and sequence comparison* - The 37 structures of MGL available on Protein Data Bank [36] were downloaded and visually inspected using PyMOL (PyMOL Molecular Graphics System, Version 1.8 Schrödinger, LLC.) in order to select one crystallographic structure for each microorganism. The selection took into account chain integrity, the absence of mutations and the presence of ligands. Among them, six wild type structures were selected for further analysis (PDB ID: 4OMA, 2O7C, 3ACZ, 4U1T, 1E5F, 5DX5) [28, 29, 37]. A library of 3558 primary sequences of MGL belonging to several microorganisms was downloaded in FASTA format from RefSeq Database of NCBI Protein Data bank [38]. Only lyases whose sequence length was between 370

and 420 amino acids were selected. Redundancy in the organism name or in the amino acid sequence was avoided using a python script. At the end of this procedure, 1223 sequences were obtained. In order to reduce the number of sequences, a homology based sequence alignment was performed using the jackhmmer program included in HMMER3 suite [39]. This iterative protein search used as query the protein sequences belonging to the six microorganisms whose crystal structure was present in Protein Data Bank. The protein database was formed by the 1223 sequences without the sequence under analysis. The first 100 homologous sequences for each of the six query proteins were merged and the sequences that appeared more than once were removed. A library containing 354 sequences was generated. The alignment of these sequences was performed with ClustalO algorithm included in Seaview 4 program [40, 41] available for ubuntu 16.4 operating system. The residue conservation analysis was performed with ConSurf server [42-44] for each crystallographic structure. Results were visualized and inspected with PyMOL.

2.3. *Site-saturation mutagenesis* - Site-saturation mutagenesis was carried out at four independent amino acid positions by using the QuikChange II XL site-directed mutagenesis kit (Agilent Technologies, Santa Clara, CA, USA) with the recombinant expression vector pET-mgl containing the wild type *mgl* gene [45] as a template, as detailed in [34]. The mutation is introduced in a single PCR with one pair of complementary degenerate synthetic primer (Table S1). All primers were synthesized and purified by Eurofins Genomics (Ebersberg, Germany). For all primers, randomized positions are in boldface with N = A/C/G/T (Table S1). The PCR amplifications were carried out with PfuUltra High Fidelity DNA polymerase (Agilent Technologies, Santa Clara, CA, USA). The 50 µl PCR reaction mixture was carried out with 50 ng template, 2.5 U of PfuUltra High Fidelity DNA polymerase and with dNTPs and primer pair concentrations according to manufacturer's protocol. The extension reaction was initiated by pre-heating the reaction mixture at 94 °C for 1 min; 18 cycles of 94 °C for 50 s, 60 °C for 50 s and 68 °C for 9 min according to the length of template; followed by incubation at 68 °C for 10 minutes. The template DNA was eliminated by enzymatic digestion with the *Dpn*I restriction enzyme,

specific for methylated DNA. The PCR products were used to transform BL21(DE3) *E. coli* cells and grown on Luria–Bertani (LB) plate containing 100 μg/ml ampicillin overnight at 37 °C. These clones were used for the screening procedure. For each position, 282 clones were screened and 10 clones were sequenced to verify the mutagenesis efficiency.

2.4. *HTP Screening for high activity MGL variants* - The mutant libraries obtained from site-saturation mutagenesis were screened by a rapid colorimetric assay based on the determination of 2-ketobutyryl 2,4-dinitrophenylhydrazone performed with an automated liquid-handler system (epMotion 5075, Eppendorf, Hamburg, Germany) [34, 46]. Single recombinant *E. coli* cultures (1 mL, grown in DeepWell plate, Eppendorf, Hamburg, Germany) were incubated in autoinduction medium [47] at 37 °C for 24 h. An aliquot (200 μL) of each culture was transferred to a 96-well microtiter plate. Cell lysis was performed by adding 50 μL of lysozyme to a final concentration of 0.5 mg/ml. The catalytic activity was assayed on the crude extract by adding the substrate (25 mM L-Met final concentration) and incubating the plates at 37 °C for 20 minutes. Then, 2,4-dinitrophenylhydrazine reagent (1 mM DNPH in 1 M HCl) was added to a final concentration of 0.3 mM, and incubated at 37 °C for 10 min. The α-ketobutyrate is derivatized to a phenylhydrazone. The color of the phenylhydazone is developed by adding NaOH to a final concentration of 0.4 M. The absorbance of the mixture was measured at 450 nm by a microtiter plate reader (Sunrise, Tecan, U.K., Goring-on-Thames, U.K.) and compared to cultures expressing the wild type MGL. The variants that outperformed the control were selected for further characterization. Mutations were confirmed by automated DNA sequencing carried out by Microsynth GmbH (Balgach, Switzerland).

2.5. *Enzyme expression and purification* - *E. coli* BL21(DE3) cells containing the plasmid with the gene of mutant *C. freundii* MGL were grown and the enzyme was purified according to the protocol used for wild type [48]. The concentration of homogeneous protein was determined by the absorbance at 278 nm ($\varepsilon^{0.1\%}_{278}$ = 0.8) [49]. Protein purity was assessed by SDS-PAGE under

denaturating conditions and found to be 90%. The protein was stored at -80 °C in buffer 100 mM potassium phosphate (pH 8.0), 1 mM EDTA, 5 mM DTT, 100 μM PLP.

2.6. *Activity assay* - MGL activity was determined using L-methionine as a substrate by measuring the rate of α-ketobutyrate production in the coupled reaction with HO-HxoDH monitoring the decrease of NADH absorption at 340 nm ($\Delta\varepsilon$ = 6220 $M^{-1}cm^{-1}$) at 30 °C. The reaction mixture contained 100 mM potassium phosphate, pH 8.0, 100 μM PLP, 5 mM DTT, 0.2 mM NADH, 70 U HO-HxoDH, and 30 mM L-methionine. One unit of enzyme activity is defined as the amount of the enzyme that catalyzes the formation of 1.0 μmol min^{-1} of α-ketobutyrate at pH 8.0, 30 °C.

2.7. *Determination of the steady state parameters of the* α,γ*-elimination reaction* and *the* α,β*-elimination reaction* - The steady state parameters of the α,γ-elimination reaction were determined by the rates of α-ketobutyrate formation in a coupled reaction with HO-Hxo-DH [50] under the conditions described above at pH 7.2, 30 °C, by varying the substrate concentration in the reaction mixture. The steady state parameters of the α,β-elimination reaction were determined by the rates of pyruvate formation in a coupled reaction with lactate dehydrogenase under the conditions described above at pH 7.2, 30 °C, by varying the substrate concentration in the reaction mixture. Data were processed according to the Michaelis–Menten equation. The molecular mass of the enzyme subunit, 43 kDa, was used in the calculations.

2.8. *Circular dichroism* - All samples were prepared at a protein concentration of 3 μM (protomer concentration) in a buffer containing 100 mM potassium phosphate, pH 7.4. CD spectra were recorded at 25 °C with a Jasco J-715 spectropolarimeter equipped with a Peltier temperature control unit (Jasco Easton, MD, USA). The far-UV measurements were recorded from 190 to 260 nm using a path length of 1 mm and the spectra obtained were the average of five scans at a scan rate of 50 nm/min. The buffer contribution was subtracted from the final spectra.

2.9. *Absorbance and fluorescence measurements* - Absorption spectra were carried out using a double beam Cary4000 UV/Vis spectrophotometer (Agilent Technologies, Santa Clara, CA, USA). Fluorescence measurements were performed using a Fluoromax-3 spectrofluorometer (Horiba Jobin Yvon, Milan, Italy). Excitation wavelengths of 295 nm, 330 nm and 415 nm were used, with an excitation and emission slit width of 3-5 nm. All spectra were corrected for buffer contribution. Measurements were carried out at 20 °C in 100 mM potassium phosphate, pH 7.4, at 13 μM MGL (protomer concentration).

2.10. *Evaluation of in vitro cytotoxicity by MTS assay* - The cytotoxic activity was evaluated for the human prostate (PC-3), mammary gland (MCF7), colon (HT29) adenocarcinoma and human skin fibroblast (Hs27) cell lines. In the exponential growth phase, cells were seeded at 5 x 10^4/mL into 96-well flat bottom microplates. Cells were cultured in DMEM supplemented with 5% FBS, 1% L-glutamine and 1% penicillin/streptomycin at 37 °C and 5% CO_2. After 24h from seeding, wild type and V358Y MGL contained in a sterile PBS solution, pH 7.4, were added to DMEM medium supplemented with 5% FBS and 0.5 mM PLP in PBS and co-incubated for 72 h. Enzyme concentrations in the culture medium were in the range 0.0005–0.5 mg/mL. An equal volume of PBS with 0.5 mM PLP was added to DMEM medium in the control wells. The anti-proliferative activity was evaluated by a colorimetric assay (CellTiter96R Aqueous One Solution Cell Proliferation Assay, Promega Corporation, Madison, WI, USA). A small amount of CellTiter96R AQueous One Solution Cell Proliferation Assay was added directly to culture wells, incubated for 4 h and then the absorbance recorded at 450 nm with a 96-wells plate reader (SPECTRAFluor, Tecan U.K., Goring-on-Thames, U.K.). Cytotoxicity experiments were carried out in quadruplicate.

2.11. *Crystallization and data collection* - Crystals of V358Y MGL were obtained at 30°C by the hanging drop vapor diffusion at the same conditions as described [24] using 35% (w/v) polyethylene glycol monomethyl ether (MMEPEG) 2000 as the precipitant. Rhombic crystals grew up to 0.3-0.4 mm dimension within 10 days.

Diffraction data were collected at the Elettra XRD1 beamline (Trieste, Italy) using Pilatus 2M (Dectris) detector and processed by XDS program [51]. Crystals belonged to the space group *I222* with unit cell parameters a = 56.67 Å, b = 122.87 Å, c = 127.52 Å, α=β=γ=90° and contained one subunit in an asymmetric unit. Detailed data collection statistics are shown in Table 1.

Table 1. Data collection and refinement statistics. Values in parentheses are for the highest resolution shell. $CC_{1/2}$ is the Pearson's correlation coefficient calculated for I_{mean} by splitting the data randomly in half by AIMLESS/SCALA [52].

Space group	*I222*
Unit cell parameters (Å)	a = 56.67 Å, b = 122.87 Å, c = 127.52 Å $\alpha = \beta = \gamma = 90°$
Wavelength (Å)	1.00
Resolution (Å)	50-1.45 (1.50-1.45)
Completeness (%)	99.47 (99.7)
Redundancy	2.25 (2.36)
R_{merge} (%)	0.026 (0.434)
R_{meas} (%)	0.037 (0.614)
Mean((I)/sd(I))	7.2 (2.0)
CC(1/2)	0.999 (0.837)
Disordered protein residues	1, 398
No. of non-H protein atoms	3635
No. of water atoms	383
No. of unique reflections	78624
R/ R_{free}	0.138/0.174 (0.214/0.266)
R_{free} test set reflections	3915 (4.98%)
Mean temperature factor B (Å^2)	26.00

R.m.s. deviation from ideal values	
Bond lengths (Å)	0.005
Bond angles (°)	0.844
Chirality angles (°)	0.079
Planar angles (°)	0.006
Ramachandran plot	
Favoured region (%)	97.64
Allowed region (%)	1.77
Outlier region (%)	0.59 [S190, K210] †

† The conformation of the amino acid residues at this position is a characteristic feature of the protein [24].

2.12. *X-ray structure determination and refinement* - The structure was solved by molecular replacement using the structure of *C. freundii* MGL (PDB code 2RFV) by rigid body procedure, implemented in PHASER of the CCP4 software suite [53]. Flexible loops of the protein and water molecules were removed from the initial model to exclude model bias during the first round of refinement. The model was improved using manual rebuilding with COOT [54] and maximum likelihood refinement using REFMAC5 [55]. An excess of electron density at the sulfur atom of C4 and C115 forced us to change these residues to 3-sulfenoalanine. The final step of the structure refinement was performed to 1.45 Å using the phenix.refine procedure implemented in the PHENIX suite [56] with R_{work} of 13.8% and R_{free} of 17.4% (Table 1). The final model contains 3635 non-hydrogen atoms including the internal aldimine, two molecules of MMEPEG 2000 and 346 water molecules. The structure was submitted to the Protein Data Bank with PDB code 6EGR and validated.

3. RESULTS AND DISCUSSION

3.1. Identification of "hot spots" for MGL engineering by phylogenetic analysis - The integration of sequence and structure-based analysis in protein engineering is a powerful approach for the identification of residues affecting the functional properties. The positions more prone to accommodate diversity are good targets for site-saturation mutagenesis. Such a design strategy possesses the advantage of an increased probability of beneficial mutations combined with a significant reduction of the library size. The degree of amino acid variation was performed using the NCBI protein databank, filtered for MGL-containing organisms available in Refseq database. Only lyases were selected and the chain length cut-off was set between 370 and 420 amino acid. These sequences were parsed to remove redundancy. The resulting 1223 sequences were used to perform a homologues search using as query each of the six MGL sequences from microorganisms whose 3D structures are deposited in the Protein Data Bank: *Citrobacter freundii* (UniProtKB AC: Q84AR1), *Pseudomonas putida* (UniProtKB AC: P13254), *Entamoeba histolytica* (UniProtKB AC: Q86D28), *Trichomonas vaginalis* (UniProtKB AC: O15564), *Micromonospora echinospora* (UniProtKB AC: Q8KNG3) and *Clostridium sporogenes* (UniProtKB AC: J7TA22). Following filtering to remove duplicates, 354 different protein sequences were obtained, aligned and used to perform the residue conservation analysis with Consurf web server. The projection of the conservation degree onto the molecular structure of MGL revealed patches of highly conserved residues localized in regions with relevant biological function such as the active site and the dimer interface (Figure S1). Not unexpectedly, the Consurf analysis shows that the residues building the active site are invariant (Figure 1a). The percentage of residue conservation for amino acids positioned within a 8 Å sphere centered on the PLP is reported in Table 2. Furthermore, also residues at the dimer interface show high Consurf conservation scores (Figure 1b, Table 2) because hydrogen bonds and electrostatic interactions stabilize the dimeric unit.

(a)

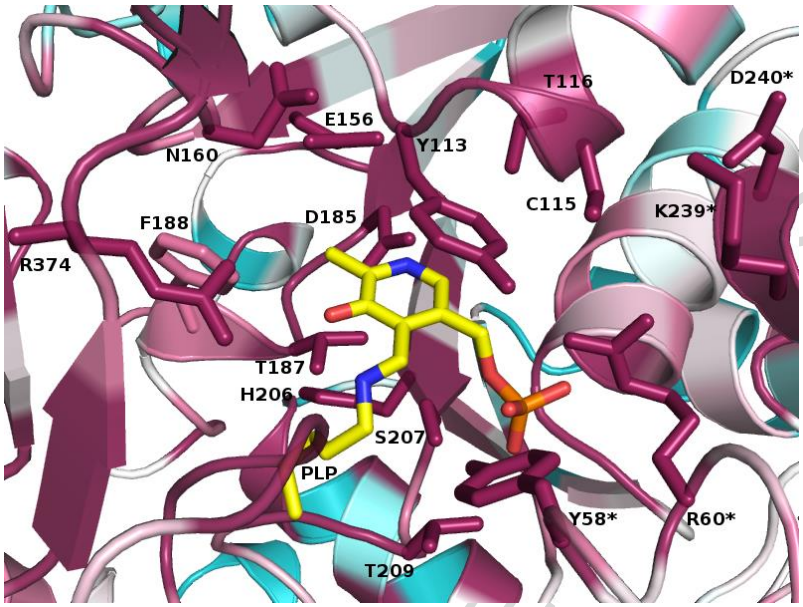

(b)

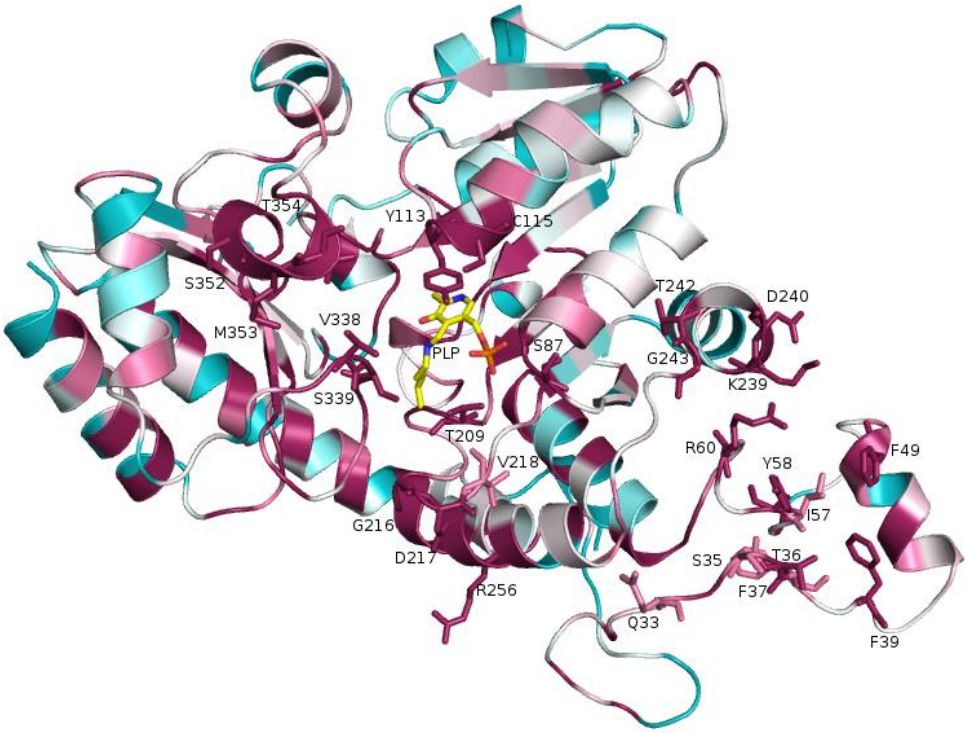

Figure 1. (a) Residues of *C. freundii* MGL active site in a 8 Å shell from PLP (Consurf coloring – PLP in yellow). Asterisks mark residues belonging to the second subunit of the active dimer. (b) Residues of *C. freundii* MGL protomer involved in the dimer interface (Consurf coloring – PLP in yellow).

Table 2. Amino acid conservation analysis of MGL. The percentage was obtained from the Consurf analysis of 354 proteins.

Active site	%		%		%
Y58	100	E156	100	T209	99.7
R60	100	N160	100	K210	100
G88	100	D185	100	S339	100
Y113	100	T187	100	L340	100
G114	99.7	F188	50.6	R374	100
C115	98.8	H206	99.1		
T116	99.1	S207	100		

Dimer interface	%		%		%
Q33	69.2	S87	99.7	D240	98.3
S35	68.6	Y113	100	T242	96.3
T36	99.7	C115	98.8	G243	100
F37	84.1	T209	99.7	R256	100
F39	99.7	K210	100	V338	99.7
F49	99.4	G216	98.3	S339	100
I57	57.1	D217	100	S352	95.8
Y58	100	V218	57	M353	100
R60	100	K239	98.3	T254	100
Active site channel	%		%		%
H349	99.7	H355	100	E361	83
P350	95.7	S356	93.2	E362	88.7
A351	99.7	P357	46.9	R363	91.8
S352	95.8	V358	11.9	L364	18.1
M353	100	A359	4.2	K365	16.1
T354	100	P360	54.7	A366	45.5

Differently from the active site and the dimer interface, the amino acids at the protein surface, exposed to the solvent, show a higher degree of variability (Figure 2). In particular, a stretch of amino acids following the highly conserved sequence of helix 16 (amino acids 349 – 356) is hypervariant (Figure 2, Table 2). Consurf results show that position 357 harbors a proline in 47% of the sequences, threonine in 25% and serine in 15%. At position 358, endowed with an intermediate conservation score, -0.586, valine is present in 12% of MGLs, including *C. freundii*, tyrosine in 80%, isoleucine in 3% and methionine in 2%. Proline at position 360 is substituted by lysine (10%), glutamic acid (6%), alanine (15%) and arginine (8%). Instead, residue 366 is alanine in 45% of MGLs with the main variations being histidine (37%) and methionine (3%), serine (7%) and tyrosine (4%). These very variable residues flank the entrance of the channel leading to the active

site of MGL. In the attempt to engineer enzymes, the active site is usually regarded as the obvious starting point. However, several studies proved that substitution of residues located in distal region of the protein matrix might be a successful strategy to modulate the enzyme catalytic activity, since their impact on function may be assessed without disturbing the enzyme-substrate interface and without disrupting the active site architecture [57, 58]. Thus, these four non-conserved amino acids located in the active site access channel were selected as target residues in the search for variants with improved catalytic efficiency of MGL.

(*a*)

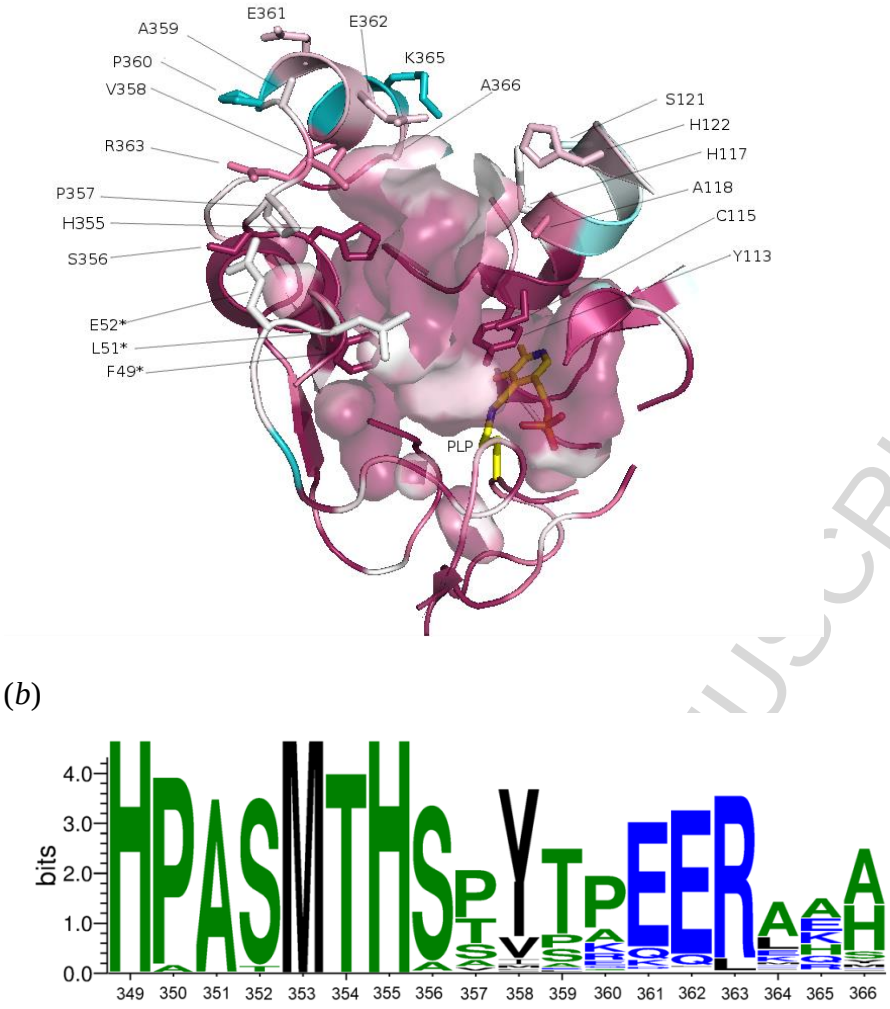

Figure 2. (*a*) Residues delimiting the access to the binding cavity (Consurf coloring of side chains – PLP in yellow). Residues of the neighboring subunit are marked with asterisks. (*b*) Sequence conservation of amino acids 349-366 of MGL generated by Weblogo plot [59]. Data for this logo consist of 354 sequences. The overall height of each stack is proportional to the sequence conservation at each position measured in bits. The relative size of each letter indicates the frequency in the sequences. Letters are ordered from the most to the least frequent amino acid. Hydrophilic amino residues are colored in blue; neutral are in green and hydrophobic in black.

Construction of site-saturation mutagenesis libraries - Site-saturation mutagenesis experiments were independently performed at positions 357, 358, 360 and 366 of *C. freundii* MGL. The α,γ-

elimination activity of the generated variant libraries was evaluated by high-throughput screening on a 96-well microtiter plate using an automated liquid-handler system. For each position, 282 clones were screened, a number that gives a probability of approximately 96% of obtaining clones possessing each single amino acid at the investigated position. The DNPH discontinuous colorimetric activity assay, described in Material and Methods, allowed selecting clones with the highest catalytic activity in the bacterial cells lysate. Ten variants with beneficial substitutions were identified by the screening procedure. Nevertheless, useful information on the substitutability, i.e. the ability to accept sequence changes without loss of function, are obtained from the percentage of inactive clones. When performing site-saturation mutagenesis at position 357 and 360, about one third of clones lost their function indicated by an absorbance intensity in the colorimetric assay less or equal to the 10% of the wild type signal. At position 358, almost half of the clones were inactive. Upon substitution at position 366, only one tenth of clones were inactive. Altogether, these data show that MGL is recalcitrant to random codon changes despite the mobility and exposure to the solvent of this loop. Because the mutations at positions 357, 358, 360, and 366 are in a mobile loop not involved in the dimer-of-dimers assembly, it is unlikely that loss of activity is caused by tetramer misassembly but may be plausibly due to protein misfolding. In turn, this finding supports the notion of a tight link between distal portions of the protein matrix and the catalytic core. Interestingly, among the novel sequence combination generated by site-saturation mutagenesis in *C. freundii* MGL, some residues have been already naturally selected and are present in protein homologous sequences. In particular, the randomly selected Tyr exhibits a high frequency of occurrence at position equivalent to 358 in other species, especially those endowed with high catalytic activity (see below). In addition, the variant P360K identified by the library screening introduces in *C. freundii* the amino acid present at the equivalent position in *T. vaginalis*, *C. novyi* and *C. tetani*, while Y366 is the amino acid present in *P. putida* at the equivalent position.

All ten variants identified by the screening procedure were expressed in BL21(DE3) *E. coli* cells and purified. For all, the expression yield was similar to the wild type enzyme, i.e. about 60 mg/L.

An increase in the specific activity for the α,γ-elimination reaction of L-Met, using the D-2-hydroxyisocaproate dehydrogenase (HO-Hxo-DH) coupled assay, was observed for seven of the ten purified variants (Figure S2). The kinetic parameters (k_{cat} and K_M values) were determined for the most active variants of MGL at each position and compared to the values of the wild type (Table 3). A 1.9-fold increase in k_{cat} was measured for V358Y, while all other variants showed comparable k_{cat} with respect to the wild type. All variants showed an increased K_M resulting in a decreased catalytic efficiency (k_{cat} /K_M). This finding further supports a long distance effect brought about by single amino acid replacement of channel-lining residues possibly via alteration of the conformational landscape.

Table 3. Kinetic parameters of MGL mutants in the α,γ-elimination reaction with L-methionine. The rate of α-ketobutyric acid production was measured in a coupled assay at 30 °C. The reaction mixture contained 100 mM potassium phosphate, 100 μM PLP, 5 mM DTT, 0.2 mM NADH, pH 7.2.

MGL	k_{cat} (s^{-1})	K_M (mM)	k_{cat}/K_M ($M^{-1}s^{-1}$)
wild type	7.9 ±0.3	0.8±0.1	$9.7x10^3$
P357I	9.0±0.3	3.7±0.4	$2.4x10^3$
V358Y	15.1±0.6	2.7±0.3	$5.6x10^3$
P360Q	7.4±0.4	1.6±0.3	$4.6x10^3$
A366Y	8.0±0.7	5.5±1.3	$1.5x10^3$

A more detailed characterization of the catalytic properties was carried out for MGL V358Y, the variant that showed a higher catalytic rate. Specifically, the kinetic parameters were determined for

C. freundii wild type MGL and MGL V358Y using different substrates that undergo the α,γ-elimination (methionine and homocysteine) and/or α,β-elimination (S-methyl-L-cysteine and cysteine) (Table 4).

Table 4. Kinetic parameters of *C. freundii* MGL V358Y in the α,γ-elimination and α,β-elimination reaction with different substrates. The rate of α-ketobutyric acid or pyruvate production was measured in a coupled assay, at 30 °C, for the α,γ-elimination and α,β-elimination, respectively. The reaction mixture contained 100 mM potassium phosphate, 100 μM PLP, 5 to 10 mM DTT, 0.2 mM NADH, pH 7.2.

	C. freundii MGL wild type			*C. freundii* MGL V358Y		
	k_{cat} (s^{-1})	K_M (mM)	k_{cat}/K_M ($M^{-1}s^{-1}$)	k_{cat} (s^{-1})	K_M (mM)	k_{cat}/K_M ($M^{-1}s^{-1}$)
L-methionine	7.9±0.3	0.8±0.1	$9.7x10^3$	15.1±0.6	2.7±0.3	$5.6x10^3$
D,L-homocysteine	3.5±0.2	1.1±0.2	$3.2x10^3$	7.8±0.5	2.2±0.4	$3.5x10^3$
S-methyl-L-cysteine	2.2±0.1	0.8±0.2	$2.7x10^3$	5.1±0.1	3.3±0.3	$1.5x10^3$
cysteine	1.5±0.1	0.3±0.1	$5.0x10^3$	2.1±0.1	0.6±0.1	$3.5x10^3$

For the wild type MGL, the catalytic parameters are similar to those previously determined using a discontinuous assay for the α,γ-elimination and a continuous assay for the α,β-elimination [48]. The variant V358Y exhibits consistently a two-fold increase in the catalytic rate for all analyzed

substrates as well as a two- to three-fold increase in the K_M resulting in catalytic efficiencies equal or lower than the wild type enzyme. This finding suggests that the K_M values might not represent the affinity between substrate and enzyme but rather reflect the increase in k_{cat}. Under this assumption, K_M, that following the Michaelis-Menten model is equal to:

$$K_M = (k_{cat} + k_{-1})/k_1 \qquad \text{eq. 1}$$

where k_1 and k_{-1} are the rate constants for the formation and disappearance of the enzyme-substrate complex, can be approximated to

$$K_M = k_{cat}/k_1 \qquad \text{eq. 2}$$

according to the model proposed by Van Slyke-Cullen for irreversible reactions [60]. The rate constant in eq. 2 is, thus, an "apparent" bimolecular association rate constant, mathematically equivalent to the specificity constant [61]. It is worthy to point out that the V358Y mutant displays similar effects, i.e. simultaneous increase in k_{cat} and K_M on different substrates and with different catalytic mechanisms (α,γ elimination and α,β elimination). The increase in k_{cat} caused by V358Y mutation is not easily explained based on differences in the three dimensional structure or in the conformational flexibility (see below). Thus, one may assume that the higher k_{cat} value for the variant enzyme is due to an acceleration of a specific step(s) of the reaction after aminocrotonate formation or in products release. Earlier, we suggested [29] that a movement of C-terminal region of *C. freundii* MGL may assist the egress of the products of the physiological reaction. Therefore, mutations that affect loop mobility or disorder-to-order rearrangement alter the conformational landscape and the catalytic parameters.

3.2. Spectroscopic characterization of V358Y MGL - Circular dichroism spectra were recorded for V358Y and compared to wild type MGL (Figure 3*a*). The spectrum shows two minima at 208

and 222 nm, typical of proteins with a high helical content. Estimation of the percentages of protein secondary structure calculated with K2D (Dichroweb) from far-UV circular dichroism spectra of the variant enzyme indicates a small change in secondary structure content. The UV-visible absorption spectrum of V358Y is similar to that of the wild type enzyme (Figure 3*b*). It is characterized by the typical protein band at 280 nm and a prominent band centered at 420 nm, assigned to the ketoenamine form of PLP. The band at 330 nm, attributed to the enolimine tautomer of the Schiff base of PLP [49], is less pronounced suggesting a shift of the enolimine-ketoenamine equilibrium towards the latter. The protein fluorescence emission spectra of MGL obtained upon excitation at 295 and 415 nm are reported in Figure 3*c*-*d*. The tryptophan fluorescence spectrum exhibits an emission maximum slightly blue shifted and less intense with respect to the wild type (Figure 3*c*). As previously reported [35], this emission originates from the single Trp252 located in a partially apolar environment. The blue shift might be associated to a small conformational change, as hinted by the circular dichroism data. The coenzyme fluorescence spectrum upon excitation at 330 nm, the wavelength where the PLP enolimine tautomer absorbs, exhibits a slightly blue shifted and less intense band (data not shown). When MGL is excited at 415 nm, the wavelength where the ketoenamine tautomer of PLP absorbs, an emission band centered at 494 nm is observed (Figure 3*d*), more intense for the mutant with respect to wild type. Overall, the spectroscopic properties of V358Y are slightly altered by the amino acid substitution, indicating that in spite of the distant positioning of tyrosine from the PLP binding site the cofactor microenvironment and the active site architecture are slightly perturbed.

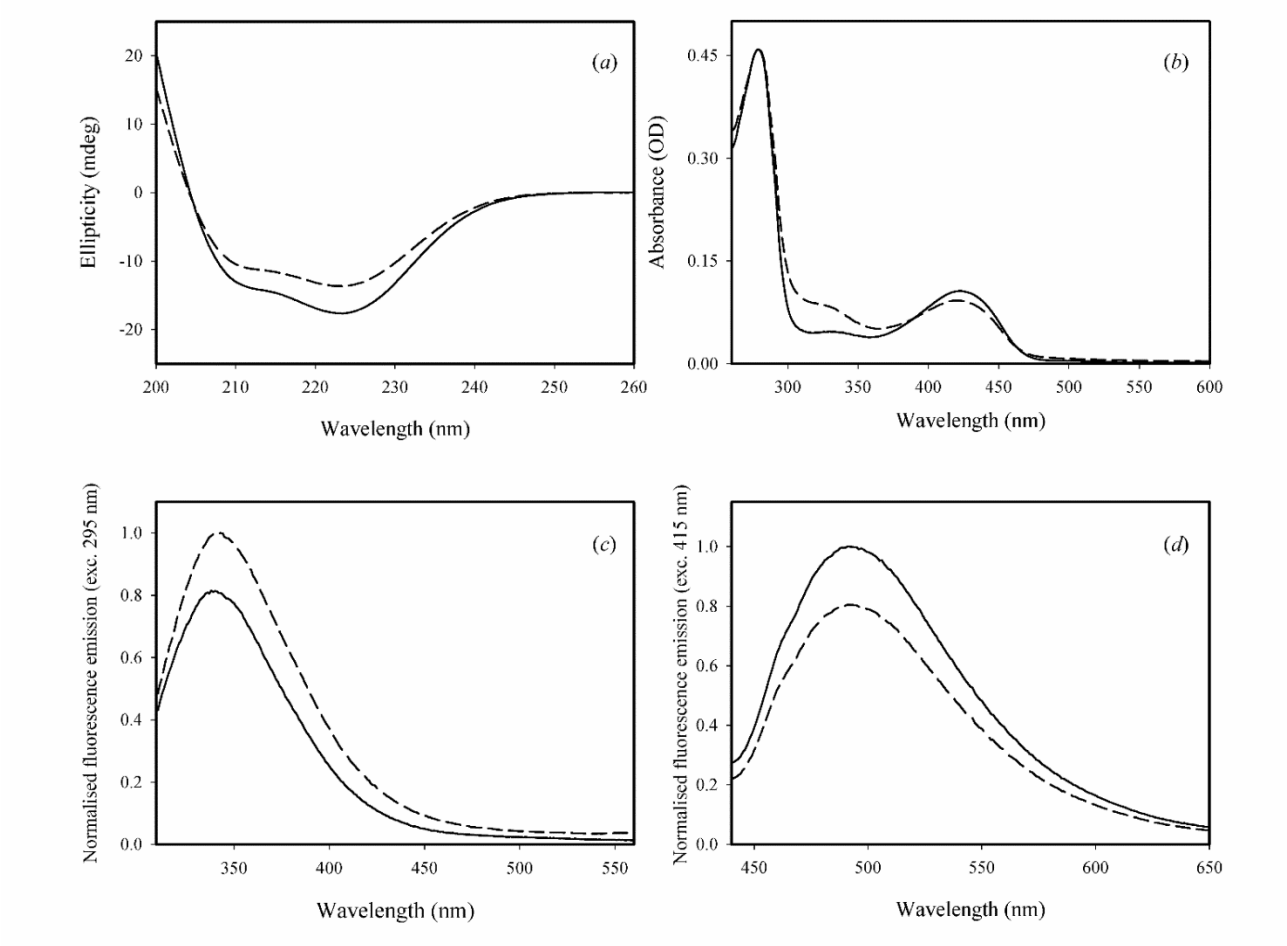

Figure 3. Comparison of the spectroscopic properties of V358Y (solid line) and wild type (dashed line) MGL. (*a*) CD spectra in 100 mM potassium phosphate pH 7.4. (*b*) Absorption spectra. (*c*) Fluorescence emission spectrum upon excitation at 295 nm (slit 3 nm). (*d*) Fluorescence emission spectrum upon excitation at 415 nm (slit 5 nm).

3.3. Cytotoxicity of V358Y MGL - We quantified the antiproliferative effect of V358Y MGL on normal and cancer cells by MTS cytotoxicity assay. Specifically, we tested prostate (PC-3), breast (MCF7), and colon adenocarcinoma (HT29) cell lines. Healthy dermis fibroblasts (Hs27) were used as a control. V358Y MGL selectively inhibits cancer cell growth with a half-maximal inhibitory concentration (IC_{50}) almost two-fold lower than the wild type MGL (Table 5). This finding is quite encouraging, even if the decrease in IC_{50} may not be a sole consequence of the increased k_{cat} since

other factors, such as enzyme stability, coenzyme affinity, resistance to oxidation and proteolysis, might play a role. Furthermore, a full understanding of the mechanisms triggered by methionine depletion has not yet been reached. Upon methionine deprivation, cancer cell are reported to arrest in the S/G_2 phase of the cell cycle and to be susceptible to spontaneous death and hypersensitive to chemotherapeutic agents [62, 63]. Based on our preliminary experiments, the mechanism of cell death is not via apoptosis.

Table 5. Comparison of cytotoxicity activity (IC_{50}) of V358Y and wild type *C. freundii* MGL on normal and cancer cell lines.

	Prostate adenocarcinoma (PC3)	***Breast adenocarcinoma (MCF7)***	***Colon adenocarcinoma (HT29)***	***Fibroblasts (Hs27)***
wild type	37±7 μg/ml	33±1 μg/ml	34±2 μg/ml	>250 μg/ml
V358Y	22±3 μg/ml	17±1 μg/ml	17±1 μg/ml	>250 μg/ml

3.4. X-ray structure of V358Y MGL - The crystal structure of the V358Y variant was solved at 1.45 Å resolution. The structural features of V358Y holoenzyme are similar to those of wild type holoenzyme and of the complexes of the wild type enzyme with inhibitors [27, 29] and substrates [25]. The crystals exhibit the same space group of symmetry *I*222 and contain one protomer in an asymmetric unit (Table 1). As for the wild type enzyme, V358Y is a tetramer, which consists of two catalytic dimers with the active sites formed by residues from two neighboring subunits [23] (Figure

S3*a*). Flexible regions previously identified in wild type MGLs are also found in the structure of V358Y: the long flexible N-terminal loop (residues 47-63) and two C-terminal regions (residues 160-163 and 353-368) (Figure S3*b*) [27]. These regions are located in the proximity of the active sites. With the exclusion of these flexible regions, the overall fold of the polypeptide chains of V358Y and wild type MGL (PDB code 2RFV) is almost identical (root-mean-square deviations of main chain atoms are 0.14 $Å^2$). The positions of amino acids forming the active site as well as the PLP site are the same in V358Y and in previously determined structures of *C. freundii* MGL. However, four active site residues have alternative positions in V358Y. The displacement of three of them is the result of the interconnected movement of residues N160, F188 and R374 (Figure S4). N160 is highly conserved in MGL from different sources (Table 2) [48] and is structurally invariant in a number of PLP-dependent enzymes of type I fold [18]. Movement of N160 is important for effective substrate binding and abstraction of the Cα-proton from the external aldimine [27]. The position of R374 side chain also varies (Figure S3). This flexibility allows R374 to "catch" and orient the substrate at the active sites. Due to the movement of N160 and/or R374, the ring of F188 is forced to shift downward towards the hydrophobic region formed by L163, M189 and I313. F188Y substitution in *C. freundii* MGL lowers the α,γ-elimination activity (Demidkina, unpublished results). Thus, it is likely that a tyrosine at position 188 may limit mobility of N160 and preclude its involvement in catalysis. Noteworthy, tyrosine at the equivalent position in *P. putida* MGL is located near E156 and N160 and occupies a slightly different position. C115 is the fourth residue showing two conformations in V358Y. This residue is conserved in most heterologous MGLs. It provides efficient L-methionine binding [28] and assists α,γ-elimination [4, 64]. It is an “accessible” cysteine, which can be modified by allicine to S-allylmercaptocysteine [64]. In V358Y crystal structure, C115 is oxidized to 3-sulfenoalanine. Since V358Y efficiently catalyzes L-methionine decomposition, it is plausible that C115 oxidation occurs during crystallization or is the result of the damage induced by X-ray radiation during data collection at the

synchrotron. We previously observed 3-sulfenoalanine at 115 position in the structure of wild type MGL with external enolimine with ammonia (PDB code 3MKJ).

3.5. Conformational effect of V358Y substitution - Residue 358 belongs to the unstructured part of the C-terminal highly flexible region 353-368. Comparison of MGLs structures from different sources confirms flexibility of this region (Figure 4*a*). This region makes no contacts with the rest of the protein matrix, does not interact with the other wall of the channel (residues 111-114) and is exposed to the solvent (Figure S3*a*). Despite flexibility, the 353-368 mobile region occupies a similar position in all the determined X-ray structures of *C. freundii* MGL. In this region, the largest deviation (~2 Å with respect to wild type holoenzyme) is calculated for V358Y and S339A (PDB code 5D5S) structures (Figure S3*c*).

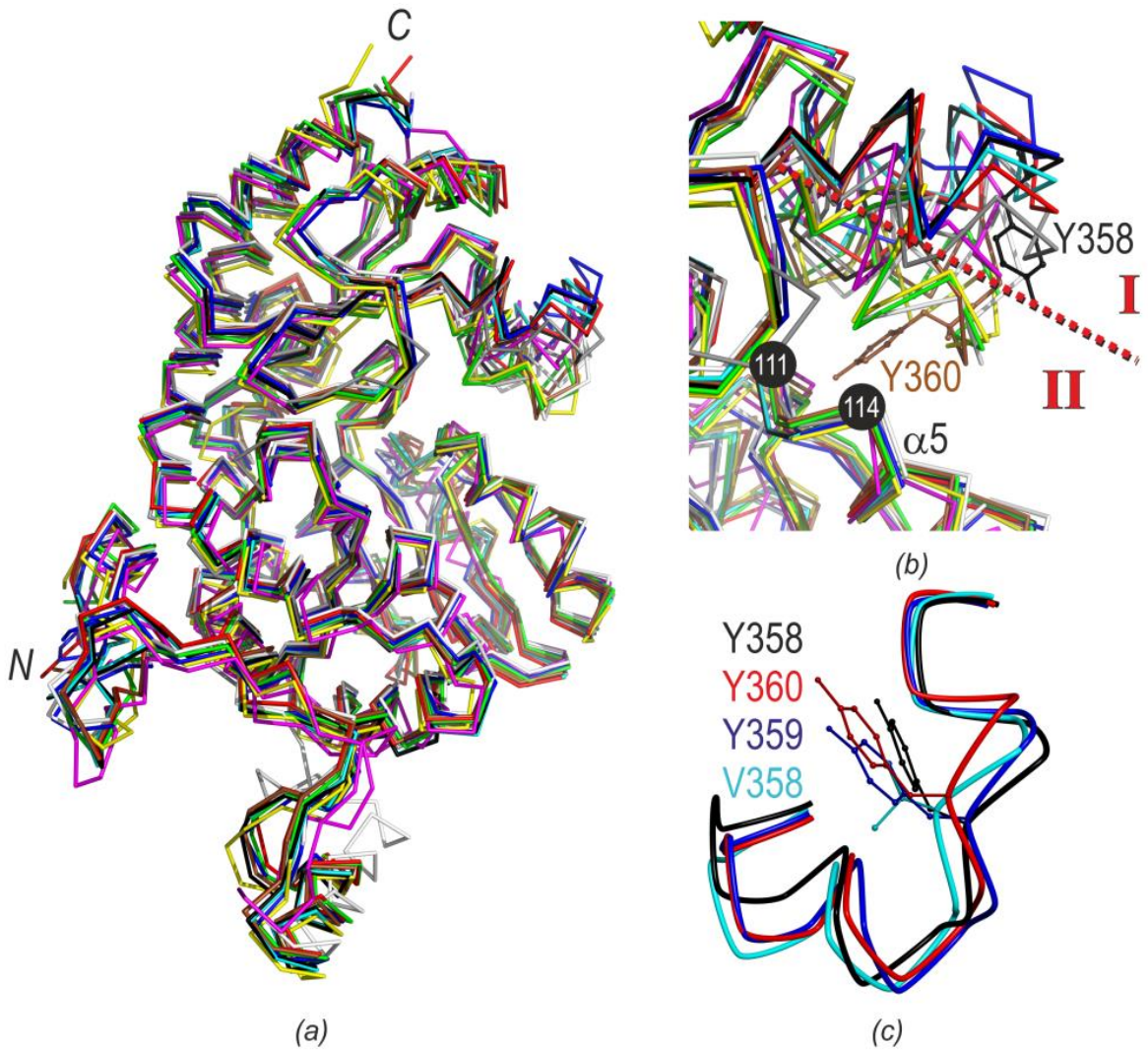

Figure 4. Superposition of the C^{α} traces of MGLs from various species. *C. sporogenes* MGL (PDB code 5DX5) chain A is in red and chain B is in brown. *C. freundii* MGL (PDB code 2RFV) is in cyan and V358Y MGL (PDB code 6EGR) is in black. *T. vaginalis* MGL is in green (PDB code 1E5F) and is in gray (PDB code 1PFF). *E. histolytica* MGL (PDB code 3ACZ) is in yellow and *M. echinospora* MGL (PDB codes 4U1T) is in magenta. *P. putida* MGL is in blue (PDB code 2O7C) and is in white (PDB code 5X2X). (*a*) Overall structure of MGLs. (*b*) C-terminal mobile region, I is marked for "open" and II for "closed" conformation of active site. (*c*) Superposition of V/Y358 of *C. freundii* MGL and corresponding tyrosine in the structure of *P. putida* and *C. sporogenes*.

Depending on the position of the 353-368 loop, MGLs structures can be classified with either an "open" or "closed" access to the active site (Figure 4*b*). All structures of *C. freundii* MGL belong to group I ("open" conformation) with the region 353-368 freely exposed to the solvent. Y358 points towards the solvent and has poor electron density (about 0.6σ for part of the side chain). F49* from the neighboring subunit of the catalytic dimer is the nearest residue at a distance of about 7Å (Figure 5*a*). Besides *C. freundii* MGL, most structures of *P. putida* MGL, one structure of *T. vaginalis* MGL (PDB code 1PFF) and *C. sporogenes* MGL (chain A, PDB code 5DX5) belong to this group. Structural alignment demonstrates that the orientation of V358 in *C. freundii* wild type MGL, Y358 in *C. freundii* V358Y MGL, Y359 in *P. putida* MGL and Y360 in *C. sporogenes* MGL (chain A) is similar (Figure 4*c*). In the structures of *M. echinospora* MGL (PDB codes 4U1T, 4U2H) this region is not detected in most of the subunits in the asymmetric unit, which contains eight protomers, whereas in other subunits (PDB codes 4U1T, chains B, F), the position is analogous to those in the structures of group I MGLs. In the "closed" conformation (group II), the region 353-368 moves towards the active site and the opposite wall of the channel and shields from the solvent the active site residues, such as Y113 and C115, which play key roles in the catalysis [28, 64]. The "closed" conformation is observed in *C. sporogenes* MGL (chain B), in two *P. putida* MGL structures (PDB codes 5X2X and 5X2Z), and in the structures of *E. histolytica* and *T. vaginalis* MGLs (PDB codes 3ACZ and 1E5F) (Figure 5b). It is noteworthy that similarly to *C. freundii* wild type MGL, the enzymes from *E. histolytica* and *T. vaginalis* exhibit valine at the corresponding position. Overall, the structural analysis does not allow concluding that the open or closed conformations are associated with the presence of a defined residue (i.e. a valine or a tyrosine) and with an effect on the catalytic activity (Figure S5, Table 6). However, the single mutation at position 358 is able to affect catalytic activity likely via a conformational rearrangement.

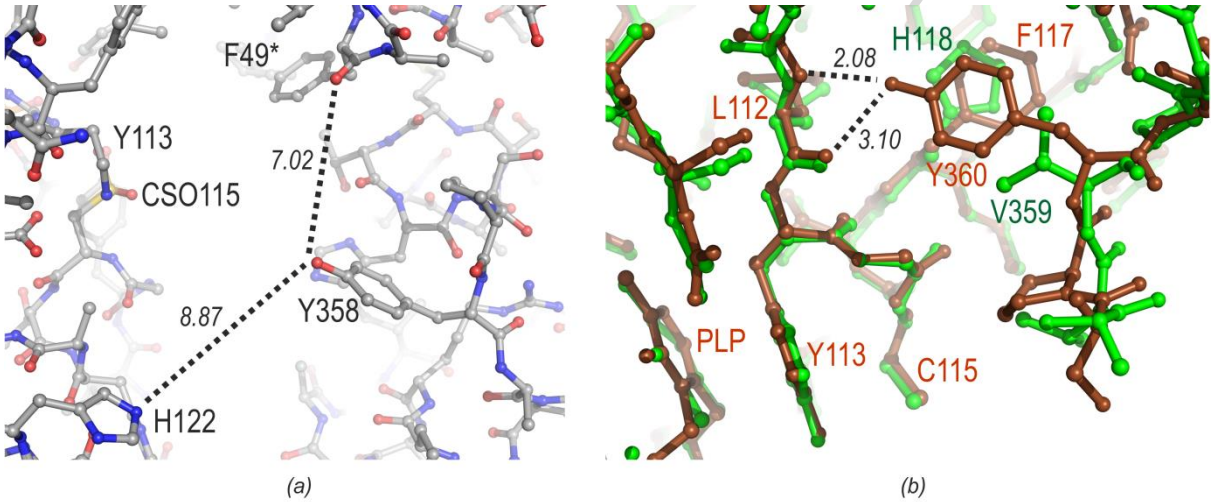

Figure 5. (*a*) Position of Y358 in the *C. freundii* V358Y MGL. Residues of the neighboring subunit are marked with asterisks. (*b*) Superposition of the *C. sporogenes* MGL (chain B; PDB code 5DX5; brown) and *T. vaginalis* MGL (PDB code 1E5F; green).

The V358Y substitution also changes the hydrophobicity profile of the substrate access pathway potentially affecting interactions that occur as the substrate or product navigate through the protein matrix. (Figure 6*a*-*b*). This, in turn, might affect the transit through the access channel, but a clear relationship between the polarity of the active site entry channel and the kinetic parameters of MGLs from different sources (especially K_M values) remains elusive (Table 6).

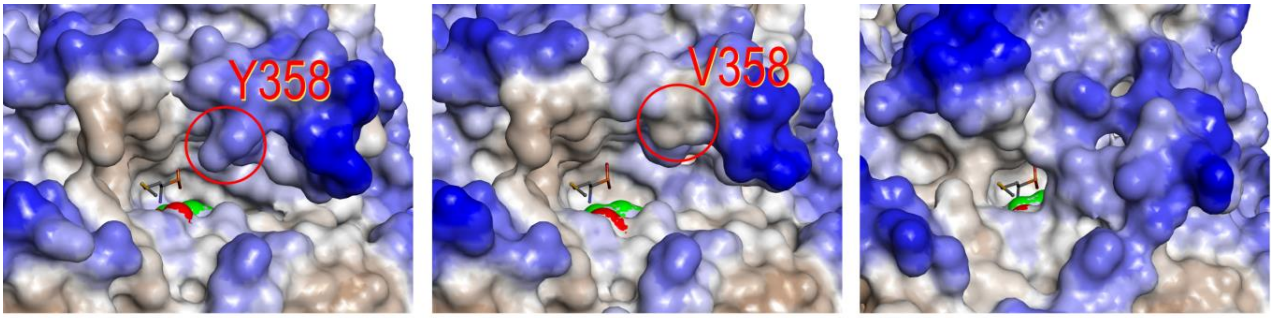

Figure 6. The catalytic dimer interface. The solvent-accessible surface is colored according to hydrophobicity profile from blue to brown with increasing hydrophobicity. The position of L-1-amino-3-methylthiopropylphosphinic acid is modeled from the structure of *C. freundii* MGL (PDB code 3JWA). Solvent-accessible surface for Y113 is in green, for C115 is in red. (*a*) *C. freundii* V358Y MGL (PDB code 6EGR) and (*b*) *C. freundii* wild type MGL (PDB code 3JWA) "open" conformation of active site; (*c*) *C. sporogenes* MGL (chain B, PDB code 5DX5) "closed" conformation.

Table 6. Comparison of the kinetic parameters of MGL from different sources.

	Residue at position 358 or corresponding	K_M (mM)	k_{cat} (s^{-1})	k_{cat}/K_M (mM^{-1} s^{-1})	Assay conditions		Ref	PDB file	UNIPROT ID
					°C	pH			
C. freundii V358Y	Y	2.7	15.1	5.6	30	7.2		6EGR (open)	
C. freundii wt	V	0.8	7.9	9.7	30	7.2	[35]	3JWA (all open structures)	Q84AR1
C. freundii wt	V	0.7	6.2	8.85	30	8	[65]		
C. sporogens	Y	0.60	21.61	36.0	30	8	[66]	5DX5 (A: open; B :closed)	J7TA22
C. novyi	Y	1.3	15.1	11.6	30	8	[67]	ND	A0A0Y0DCC0
C. tetani	Y	0.95	12	12.7	30	8	[65]	ND	Q890V5
P. putida	Y	0.5 0.90 0.92	33.4 48.6 25.3	66.8 54.0 27.6	37	8	[68] [69] [70]	all open except 5X2X and 5X2Z (closed)	P13254
M. echinospora	L	98	0.098	0.001	RT	8	[37]	4U1T (open)	Q8KNG3
T. denticola	Y	0.55	ND	ND	37	8	[71]	ND	Q73KL7
P. gingivalis	Y	1.77	3.9	2.2	30	8	[65]	ND	F5XBR2
E. hystolica Eh1 *Eh2*	V V	0.61 3.58	1.82 1.11	2.99 0.31	37	7	[72] [72]	3ACZ (closed) ND	Q86D28 Q86D27
T. vaginalis Tv1 *Tv2*	V V	0.2 10.6	6.7 0.48	38.4 0.04	37	8	[73] [48]	1E5F (closed) 1PFF (open)	O15564 O15565

4. CONCLUSIONS

With the aim of increasing the efficacy of MGL in depleting methionine from the cancer cell environment, we applied a saturation mutagenesis approach to four residues belonging to the entry channel of the active site that were shown to be variable among bacterial species and localized in a flexible C-terminal loop. Despite the distal position of these amino acids from the active site, the majority of variants were inactive or less active than the wild type enzyme, a few variants exhibited catalytic properties similar to the wild type enzyme and interestingly only one, V358Y, exhibited a 100% increase in the catalytic rate, although with a concomitant increase in K_M. If the moderate improvement in the catalytic activity of this single-site mutant may seem below expectations, it is important to underline that these results identify the flexible loop forming the entrance of the active site channel as a hot spot of the enzyme, i.e. a region comprising functionally important residues coupled to active-site dynamics that contribute to activity. This is an emerging theme in protein structure-dynamics-function relationships, as shown in recent studies [74-77].

ACKNOWLEDGEMENTS

This work was carried out with the financial support of a bilateral project between the National Research Council of Italy (CNR) (code MD P01.008), the Russian Foundation for Basic Research (RFBR) (code 15-54-78021) and the Russian Program of fundamental research for state academies for 2013-2020 years (№ 01201363820). The Interdepartmental Center for Measurements (CIM) of the University of Parma is acknowledged for CD equipment.

REFERENCES

[1] R.M. Hoffman, The wayward methyl group and the cascade to cancer, Cell Cycle, 16 (2017) 825-829.

[2] P. Cavuoto, M.F. Fenech, A review of methionine dependency and the role of methionine restriction in cancer growth control and life-span extension, Cancer Treat Rev, 38 (2012) 726-736.

[3] R.M. Hoffman, Development of recombinant methioninase to target the general cancer-specific metabolic defect of methionine dependence: a 40-year odyssey, Expert Opin Biol Ther, 15 (2015) 21-31.

[4] S.V. Revtovich, E.A. Morozova, V.V. Kulikova, N.V. Anufrieva, T.I. Osipova, V.S. Koval, A.D. Nikulin, T.V. Demidkina, Crystal structure of mutant form Cys115His of *Citrobacter freundii* methionine γ-lyase complexed with l-norleucine, Biochim Biophys Acta, 1865 (2017) 1123-1128.

[5] Y. Tan, M. Xu, R.M. Hoffman, Broad selective efficacy of recombinant methioninase and polyethylene glycol-modified recombinant methioninase on cancer cells in vitro, Anticancer Res, 30 (2010) 1041-1046.

[6] Y. Tan, M. Xu, X. Tan, X. Wang, Y. Saikawa, T. Nagahama, X. Sun, M. Lenz, R.M. Hoffman, Overexpression and large-scale production of recombinant L-methionine-α-deamino-γ-mercaptomethane-lyase for novel anticancer therapy, Protein Expr Purif, 9 (1997) 233-245.

[7] X. Sun, Z. Yang, S. Li, Y. Tan, N. Zhang, X. Wang, S. Yagi, T. Yoshioka, A. Takimoto, K. Mitsushima, A. Suginaka, E.P. Frenkel, R.M. Hoffman, In vivo efficacy of recombinant methioninase is enhanced by the combination of polyethylene glycol conjugation and pyridoxal 5'-phosphate supplementation, Cancer Res, 63 (2003) 8377-8383.

[8] T. Takakura, A. Takimoto, Y. Notsu, H. Yoshida, T. Ito, H. Nagatome, M. Ohno, Y. Kobayashi, T. Yoshioka, K. Inagaki, S. Yagi, R.M. Hoffman, N. Esaki, Physicochemical and pharmacokinetic characterization of highly potent recombinant L-methionine γ-lyase conjugated with polyethylene glycol as an antitumor agent, Cancer Res, 66 (2006) 2807-2814.

[9] F. Gay, K. Aguera, K. Senechal, A. Tainturier, W. Berlier, D. Maucort-Boulch, J. Honnorat, F. Horand, Y. Godfrin, V. Bourgeaux, Methionine tumor starvation by erythrocyte-encapsulated methionine gamma-lyase activity controlled with per os vitamin B6, Cancer Med, 6 (2017) 1437-1452.

[10] L. Xin, J.Q. Caot, C. Liu, F. Zeng, H. Cheng, X.Y. Hu, J.H. Shao, Evaluation of rMETase-loaded stealth PLGA/liposomes modified with anti-CAGE scFV for treatment of gastric carcinoma, J Biomed Nanotechnol, 11 (2015) 1153-1161.

[11] K. Miki, W. Al-Refaie, M. Xu, P. Jiang, Y. Tan, M. Bouvet, M. Zhao, A. Gupta, T. Chishima, H. Shimada, M. Makuuchi, A.R. Moossa, R.M. Hoffman, Methioninase gene therapy of human cancer cells is synergistic with recombinant methioninase treatment, Cancer Res, 60 (2000) 2696-2702.

[12] K. Igarashi, K. Kawaguchi, S. Li, Q. Han, Y. Tan, E. Gainor, T. Kiyuna, K. Miyake, M. Miyake, T. Higuchi, H. Oshiro, A.S. Singh, M.A. Eckardt, S.D. Nelson, T.A. Russell, S.M. Dry, Y. Li, N. Yamamoto, K. Hayashi, H. Kimura, S. Miwa, H. Tsuchiya, F.C. Eilber, R.M. Hoffman, Recombinant methioninase combined with doxorubicin (DOX) regresses a DOX-resistant synovial sarcoma in a patient-derived orthotopic xenograft (PDOX) mouse model, Oncotarget, 9 (2018) 19263-19272.

[13] K. Kawaguchi, Q. Han, S. Li, Y. Tan, K. Igarashi, T. Kiyuna, K. Miyake, M. Miyake, B. Chmielowski, S.D. Nelson, T.A. Russell, S.M. Dry, Y. Li, A.S. Singh, M.A. Eckardt, M. Unno, F.C. Eilber, R.M. Hoffman, Targeting methionine with oral recombinant methioninase (o-rMETase) arrests a patient-derived orthotopic xenograft (PDOX) model of BRAF-V600E mutant melanoma: implications for chronic clinical cancer therapy and prevention, Cell Cycle, 17 (2018) 356-361.

[14] K. Kawaguchi, K. Igarashi, S. Li, Q. Han, Y. Tan, T. Kiyuna, K. Miyake, T. Murakami, B. Chmielowski, S.D. Nelson, T.A. Russell, S.M. Dry, Y. Li, M. Unno, F.C. Eilber, R.M. Hoffman, Combination treatment with recombinant methioninase enables temozolomide to arrest a BRAF

V600E melanoma in a patient-derived orthotopic xenograft (PDOX) mouse model, Oncotarget, 8 (2017) 85516-85525.

[15] K. Kawaguchi, K. Igarashi, S. Li, Q. Han, Y. Tan, K. Miyake, T. Kiyuna, M. Miyake, T. Murakami, B. Chmielowski, S.D. Nelson, T.A. Russell, S.M. Dry, Y. Li, M. Unno, F.C. Eilber, R.M. Hoffman, Recombinant methioninase (rMETase) is an effective therapeutic for BRAF-V600E-negative as well as -positive melanoma in patient-derived orthotopic xenograft (PDOX) mouse models, Oncotarget, 9 (2018) 915-923.

[16] K. Kawaguchi, K. Miyake, Q. Han, S. Li, Y. Tan, K. Igarashi, T.M. Lwin, T. Higuchi, T. Kiyuna, M. Miyake, H. Oshiro, M. Bouvet, M. Unno, R.M. Hoffman, Targeting altered cancer methionine metabolism with recombinant methioninase (rMETase) overcomes partial gemcitabine-resistance and regresses a patient-derived orthotopic xenograft (PDOX) nude mouse model of pancreatic cancer, Cell Cycle, (2018) 1-6.

[17] T. Murakami, S. Li, Q. Han, Y. Tan, T. Kiyuna, K. Igarashi, K. Kawaguchi, H.K. Hwang, K. Miyake, A.S. Singh, S.D. Nelson, S.M. Dry, Y. Li, Y. Hiroshima, T.M. Lwin, J.C. DeLong, T. Chishima, K. Tanaka, M. Bouvet, I. Endo, F.C. Eilber, R.M. Hoffman, Recombinant methioninase effectively targets a Ewing's sarcoma in a patient-derived orthotopic xenograft (PDOX) nude-mouse model, Oncotarget, 8 (2017) 35630-35638.

[18] J.N. Jansonius, Structure, evolution and action of vitamin B6-dependent enzymes, Curr Opin Struct Biol, 8 (1998) 759-769.

[19] P. Christen, P.K. Mehta, From cofactor to enzymes. The molecular evolution of pyridoxal-5'-phosphate-dependent enzymes, Chem Rec, 1 (2001) 436-447.

[20] P.K. Mehta, P. Christen, The molecular evolution of pyridoxal-5'-phosphate-dependent enzymes, Adv Enzymol Relat Areas Mol Biol, 74 (2000) 129-184.

[21] G. Schneider, H. Kack, Y. Lindqvist, The manifold of vitamin B6 dependent enzymes, Structure, 8 (2000) R1-6.

[22] S. Revtovich, N. Anufrieva, E. Morozova, V. Kulikova, A. Nikulin, T. Demidkina, Structure of methionine γ-lyase from *Clostridium sporogenes*, Acta Crystallogr F, 72 (2016) 65-71.

[23] D.V. Mamaeva, E.A. Morozova, A.D. Nikulin, S.V. Revtovich, S.V. Nikonov, M.B. Garber, T.V. Demidkina, Structure of *Citrobacter freundii* L-methionine γ-lyase, Acta Crystallogr F, 61 (2005) 546-549.

[24] A. Nikulin, S. Revtovich, E. Morozova, N. Nevskaya, S. Nikonov, M. Garber, T. Demidkina, High-resolution structure of methionine γ-lyase from *Citrobacter freundii*, Acta Crystallogr D 64 (2008) 211-218.

[25] S.V. Revtovich, E.A. Morozova, E.N. Khurs, L.N. Zakomirdina, A.D. Nikulin, T.V. Demidkina, R.M. Khomutov, Three-dimensional structures of noncovalent complexes of *Citrobacter freundii* methionine γ-lyase with substrates, Biochemistry (Mosc), 76 (2011) 564-570.

[26] L. Ronda, N.P. Bazhulina, E.A. Morozova, S.V. Revtovich, V.O. Chekhov, A.D. Nikulin, T.V. Demidkina, A. Mozzarelli, Exploring methionine γ-lyase structure-function relationship via microspectrophotometry and X-ray crystallography, Biochim Biophys Acta, 1814 (2011) 834-842.

[27] S.V. Revtovich, N.G. Faleev, E.A. Morozova, N.V. Anufrieva, A.D. Nikulin, T.V. Demidkina, Crystal structure of the external aldimine of *Citrobacter freundii* methionine γ-lyase with glycine provides insight in mechanisms of two stages of physiological reaction and isotope exchange of α- and β-protons of competitive inhibitors, Biochimie, 101 (2014) 161-167.

[28] D. Kudou, S. Misaki, M. Yamashita, T. Tamura, T. Takakura, T. Yoshioka, S. Yagi, R.M. Hoffman, A. Takimoto, N. Esaki, K. Inagaki, Structure of the antitumour enzyme L-methionine γ-lyase from *Pseudomonas putida* at 1.8 Å resolution, J Biochem, 141 (2007) 535-544.

[29] N.A. Kuznetsov, N.G. Faleev, A.A. Kuznetsova, E.A. Morozova, S.V. Revtovich, N.V. Anufrieva, A.D. Nikulin, O.S. Fedorova, T.V. Demidkina, Pre-steady-state kinetic and structural analysis of interaction of methionine γ-lyase from *Citrobacter freundii* with inhibitors, J Biol Chem, 290 (2015) 671-681.

[30] S. Raboni, F. Spyrakis, B. Campanini, A. Amadasi, S. Bettati, A. Peracchi, A. Mozzarelli, R. Contestabile, Pyridoxal 5-phosphate-dependent enzymes: Catalysis, conformation, and genomics, in: L. Mander, H.-W. Liu (Eds.) Comprehensive Natural Products II: Chemistry and Biology., Elsevier, Oxford, UK, 2010 pp. 273-315.

[31] R.A. Chica, N. Doucet, J.N. Pelletier, Semi-rational approaches to engineering enzyme activity: combining the benefits of directed evolution and rational design, Curr Opin Biotechnol, 16 (2005) 378-384.

[32] G.J. Williams, R.D. Goff, C. Zhang, J.S. Thorson, Optimizing glycosyltransferase specificity via "hot spot" saturation mutagenesis presents a catalyst for novobiocin glycorandomization, Chem Biol, 15 (2008) 393-401.

[33] S. Prasad, M. Bocola, M.T. Reetz, Revisiting the lipase from *Pseudomonas aeruginosa*: directed evolution of substrate acceptance and enantioselectivity using iterative saturation mutagenesis, Chemphyschem, 12 (2011) 1550-1557.

[34] E. Rosini, L. Piubelli, G. Molla, L. Frattini, M. Valentino, A. Varriale, S. D'Auria, L. Pollegioni, Novel biosensors based on optimized glycine oxidase, FEBS J, 281 (2014) 3460-3472.

[35] E.A. Morozova, V.V. Kulikova, S. Faggiano, S. Raboni, E. Gabellieri, P. Cioni, N.V. Anufrieva, S.V. Revtovich, T. Demidkina, A. Mozzarelli, Soluble and nanoporous silica gel-entrapped *C. freundii* methionine γ-lyase, J Nanosci Nanotechnol, 18 (2018) 2210-2219.

[36] P.W. Rose, A. Prlic, A. Altunkaya, C. Bi, A.R. Bradley, C.H. Christie, L.D. Costanzo, J.M. Duarte, S. Dutta, Z. Feng, R.K. Green, D.S. Goodsell, B. Hudson, T. Kalro, R. Lowe, E. Peisach, C. Randle, A.S. Rose, C. Shao, Y.P. Tao, Y. Valasatava, M. Voigt, J.D. Westbrook, J. Woo, H. Yang, J.Y. Young, C. Zardecki, H.M. Berman, S.K. Burley, The RCSB protein data bank: integrative view of protein, gene and 3D structural information, Nucleic Acids Res, 45 (2017) D271-D281.

[37] H. Song, R. Xu, Z. Guo, Identification and characterization of a methionine γ-lyase in the calicheamicin biosynthetic cluster of *Micromonospora echinospora*, Chembiochem, 16 (2015) 100-109.

[38] N.A. O'Leary, M.W. Wright, J.R. Brister, S. Ciufo, D. Haddad, R. McVeigh, B. Rajput, B. Robbertse, B. Smith-White, D. Ako-Adjei, A. Astashyn, A. Badretdin, Y. Bao, O. Blinkova, V. Brover, V. Chetvernin, J. Choi, E. Cox, O. Ermolaeva, C.M. Farrell, T. Goldfarb, T. Gupta, D. Haft, E. Hatcher, W. Hlavina, V.S. Joardar, V.K. Kodali, W. Li, D. Maglott, P. Masterson, K.M. McGarvey, M.R. Murphy, K. O'Neill, S. Pujar, S.H. Rangwala, D. Rausch, L.D. Riddick, C. Schoch, A. Shkeda, S.S. Storz, H. Sun, F. Thibaud-Nissen, I. Tolstoy, R.E. Tully, A.R. Vatsan, C. Wallin, D. Webb, W. Wu, M.J. Landrum, A. Kimchi, T. Tatusova, M. DiCuccio, P. Kitts, T.D. Murphy, K.D. Pruitt, Reference sequence (RefSeq) database at NCBI: current status, taxonomic expansion, and functional annotation, Nucleic Acids Res, 44 (2016) D733-745.

[39] S.R. Eddy, Profile hidden Markov models, Bioinformatics, 14 (1998) 755-763.

[40] N. Galtier, M. Gouy, C. Gautier, SEAVIEW and PHYLO_WIN: two graphic tools for sequence alignment and molecular phylogeny, Comput Appl Biosci, 12 (1996) 543-548.

[41] M. Gouy, S. Guindon, O. Gascuel, SeaView version 4: A multiplatform graphical user interface for sequence alignment and phylogenetic tree building, Mol Biol Evol, 27 (2010) 221-224.

[42] H. Ashkenazy, S. Abadi, E. Martz, O. Chay, I. Mayrose, T. Pupko, N. Ben-Tal, ConSurf 2016: an improved methodology to estimate and visualize evolutionary conservation in macromolecules, Nucleic Acids Res, 44 (2016) W344-350.

[43] M. Landau, I. Mayrose, Y. Rosenberg, F. Glaser, E. Martz, T. Pupko, N. Ben-Tal, ConSurf 2005: the projection of evolutionary conservation scores of residues on protein structures, Nucleic Acids Res, 33 (2005) W299-302.

[44] F. Glaser, T. Pupko, I. Paz, R.E. Bell, D. Bechor-Shental, E. Martz, N. Ben-Tal, ConSurf: identification of functional regions in proteins by surface-mapping of phylogenetic information, Bioinformatics, 19 (2003) 163-164.

[45] I.V. Manukhov, D.V. Mamaeva, S.M. Rastorguev, N.G. Faleev, E.A. Morozova, T.V. Demidkina, G.B. Zavilgelsky, A gene encoding L-methionine γ-lyase is present in Enterobacteriaceae family genomes: identification and characterization of *Citrobacter freundii* L-methionine γ-lyase, J Bacteriol, 187 (2005) 3889-3893.

[46] G. Conti, L. Pollegioni, G. Molla, E. Rosini, Strategic manipulation of an industrial biocatalyst--evolution of a cephalosporin C acylase, FEBS J, 281 (2014) 2443-2455.

[47] F.W. Studier, Protein production by auto-induction in high density shaking cultures, Protein Expr Purif, 41 (2005) 207-234.

[48] I.V. Manukhov, D.V. Mamaeva, E.A. Morozova, S.M. Rastorguev, N.G. Faleev, T.V. Demidkina, G.B. Zavilgelsky, L-methionine γ-lyase from *Citrobacter freundii:* cloning of the gene and kinetic parameters of the enzyme, Biochemistry (Mosc), 71 (2006) 361-369.

[49] E.A. Morozova, N.P. Bazhulina, N.V. Anufrieva, D.V. Mamaeva, Y.V. Tkachev, S.A. Streltsov, V.P. Timofeev, N.G. Faleev, T.V. Demidkina, Kinetic and spectral parameters of interaction of *Citrobacter freundii* methionine γ-lyase with amino acids, Biochemistry (Mosc), 75 (2010) 1272-1280.

[50] S.M. Aitken, D.H. Kim, J.F. Kirsch, *Escherichia coli* cystathionine γ-synthase does not obey ping-pong kinetics. Novel continuous assays for the elimination and substitution reactions, Biochemistry, 42 (2003) 11297-11306.

[51] W. Kabsch, Xds, Acta Crystallogr D 66 (2010) 125-132.

[52] P.R. Evans, G.N. Murshudov, How good are my data and what is the resolution?, Acta Crystallogr. D, 69 (2013) 1204-1214.

[53] M.D. Winn, C.C. Ballard, K.D. Cowtan, E.J. Dodson, P. Emsley, P.R. Evans, R.M. Keegan, E.B. Krissinel, A.G. Leslie, A. McCoy, S.J. McNicholas, G.N. Murshudov, N.S. Pannu, E.A. Potterton, H.R. Powell, R.J. Read, A. Vagin, K.S. Wilson, Overview of the CCP4 suite and current developments, Acta Crystallogr D, 67 (2011) 235-242.

[54] P. Emsley, B. Lohkamp, W.G. Scott, K. Cowtan, Features and development of Coot, Acta Crystallogr. D 66 (2010) 486-501.

[55] G.N. Murshudov, P. Skubak, A.A. Lebedev, N.S. Pannu, R.A. Steiner, R.A. Nicholls, M.D. Winn, F. Long, A.A. Vagin, REFMAC5 for the refinement of macromolecular crystal structures, Acta Crystallogr D 67 (2011) 355-367.

[56] P.D. Adams, P.V. Afonine, G. Bunkoczi, V.B. Chen, I.W. Davis, N. Echols, J.J. Headd, L.W. Hung, G.J. Kapral, R.W. Grosse-Kunstleve, A.J. McCoy, N.W. Moriarty, R. Oeffner, R.J. Read, D.C. Richardson, J.S. Richardson, T.C. Terwilliger, P.H. Zwart, PHENIX: a comprehensive Python-based system for macromolecular structure solution, Acta Crystallogr. D 66 (2010) 213-221.

[57] S. Kaushik, S.M. Marques, P. Khirsariya, K. Paruch, L. Libichova, J. Brezovsky, Z. Prokop, R. Chaloupkova, J. Damborsky, Impact of the access tunnel engineering on catalysis is strictly ligand-specific, FEBS J, 285 (2018) 1456-1476.

[58] M. Pavlova, M. Klvana, Z. Prokop, R. Chaloupkova, P. Banas, M. Otyepka, R.C. Wade, M. Tsuda, Y. Nagata, J. Damborsky, Redesigning dehalogenase access tunnels as a strategy for degrading an anthropogenic substrate, Nat Chem Biol, 5 (2009) 727-733.

[59] G.E. Crooks, G. Hon, J.M. Chandonia, S.E. Brenner, WebLogo: a sequence logo generator, Genome Res, 14 (2004) 1188-1190.

[60] D.D. Van Slyke, G.E. Cullen, The mode of action of urease and of enzymes in general J. Biol. Chem, 19 (1914) 141-180.

[61] P. Kuzmic, Application of the Van Slyke-Cullen irreversible mechanism in the analysis of enzymatic progress curves, Anal Biochem, 394 (2009) 287-289.

[62] F. Poirson-Bichat, R.A. Goncalves, L. Miccoli, B. Dutrillaux, M.F. Poupon, Methionine depletion enhances the antitumoral efficacy of cytotoxic agents in drug-resistant human tumor xenografts, Clin Cancer Res, 6 (2000) 643-653.

[63] S. Yano, S. Li, Q. Han, Y. Tan, M. Bouvet, T. Fujiwara, R.M. Hoffman, Selective methioninase-induced trap of cancer cells in S/G2 phase visualized by FUCCI imaging confers chemosensitivity, Oncotarget, 5 (2014) 8729-8736.

[64] E.A. Morozova, S.V. Revtovich, N.V. Anufrieva, V.V. Kulikova, A.D. Nikulin, T.V. Demidkina, Alliin is a suicide substrate of *Citrobacter freundii* methionine γ-lyase: structural bases of inactivation of the enzyme, Acta Crystallogr D 70 (2014) 3034-3042.

[65] E.A. Morozova, V.V. Kulikova, D.V. Yashin, N.V. Anufrieva, N.Y. Anisimova, S.V. Revtovich, M.I. Kotlov, Y.F. Belyi, V.S. Pokrovsky, T.V. Demidkina, Kinetic parameters and cytotoxic activity of recombinant methionine γ-lyase from *Clostridium tetani, Clostridium sporogenes, Porphyromonas gingivalis* and *Citrobacter freundii*, Acta Naturae, 5 (2013) 92-98.

[66] N.V. Anufrieva, E.A. Morozova, V.V. Kulikova, N.P. Bazhulina, I.V. Manukhov, D.I. Degtev, E.Y. Gnuchikh, A.N. Rodionov, G.B. Zavilgelsky, T.V. Demidkina, Sulfoxides, analogues of L-methionine and L-cysteine as pro-drugs against gram-positive and gram-negative bacteria, Acta Naturae, 7 (2015) 128-135.

[67] V.V. Kulikova, E.A. Morozova, S.V. Revtovich, M.I. Kotlov, N.V. Anufrieva, N.P. Bazhulina, S. Raboni, S. Faggiano, E. Gabellieri, P. Cioni, Y.F. Belyi, A. Mozzarelli, T.V. Demidkina, Gene cloning, characterization, and cytotoxic activity of methionine γ-lyase from *Clostridium novyi*, IUBMB Life, 69 (2017) 668-676.

[68] M. Fukumoto, D. Kudou, S. Murano, T. Shiba, D. Sato, T. Tamura, S. Harada, K. Inagaki, The role of amino acid residues in the active site of L-methionine γ-lyase from *Pseudomonas putida*, Biosci Biotechnol Biochem, 76 (2012) 1275-1284.

[69] H. Inoue, K. Inagaki, N. Adachi, T. Tamura, N. Esaki, K. Soda, H. Tanaka, Role of tyrosine 114 of L-methionine γ-lyase from *Pseudomonas putida*, Biosci Biotechnol Biochem, 64 (2000) 2336-2343.

[70] D. Kudou, S. Misaki, M. Yamashita, T. Tamura, N. Esaki, K. Inagaki, The role of cysteine 116 in the active site of the antitumor enzyme L-methionine γ-lyase from *Pseudomonas putida*, Biosci Biotechnol Biochem, 72 (2008) 1722-1730.

[71] H. Fukamachi, Y. Nakano, S. Okano, Y. Shibata, Y. Abiko, Y. Yamashita, High production of methyl mercaptan by L-methionine-α-deamino-γ-mercaptomethane lyase from *Treponema denticola*, Biochem Biophys Res Commun, 331 (2005) 127-131.

[72] D. Sato, W. Yamagata, S. Harada, T. Nozaki, Kinetic characterization of methionine γ-lyases from the enteric protozoan parasite *Entamoeba histolytica* against physiological substrates and trifluoromethionine, a promising lead compound against amoebiasis, FEBS J, 275 (2008) 548-560.

[73] I.A. Moya, G.D. Westrop, G.H. Coombs, J.F. Honek, Mechanistic studies on the enzymatic processing of fluorinated methionine analogues by *Trichomonas vaginalis* methionine γ-lyase, Biochem J, 438 (2011) 513-521.

[74] H.G. Saavedra, J.O. Wrabl, J.A. Anderson, J. Li, V.J. Hilser, Dynamic allostery can drive cold adaptation in enzymes, Nature, (2018) 324-328.

[75] J. Mahita, R. Sowdhamini, Probing subtle conformational changes induced by phosphorylation and point mutations in the TIR domains of TLR2 and TLR3, Proteins, 86 (2018) 524-535.

[76] N. Rajasekaran, S. Suresh, S. Gopi, K. Raman, A.N. Naganathan, A general mechanism for the propagation of mutational effects in proteins, Biochemistry, 56 (2017) 294-305.

[77] G.R. Bowman, P.L. Geissler, Equilibrium fluctuations of a single folded protein reveal a multitude of potential cryptic allosteric sites, Proc Natl Acad Sci U S A, 109 (2012) 11681-11686.

SUPPLEMENTARY MATERIAL

Table S1. List of degenerate primer for site-saturation mutagenesis on *C. freundii* MGL with NNN randomization (N=A, C, G or T).

Pro357rev	5'-cctctggcgcaac**NNN**cgaatgtgtcatag-3'
Pro357for	5'-ctatgacacattcg**NNN**gttgcgccagagg-3'
Val358rev	5'-gttcctctggcgc**NNN**gggcgaatgtg-3'
Val358for	5'-cacattcgccc**NNN**gcgccagaggaac-3'
Pro360rev	5'-ctttaagccgttcctc**NNN**cgcaacgggc-3'
Pro360for	5'-gcccgttgcg**NNN**gaggaacggcttaaag-3'
Ala366rev	5'-ccgtcggtaatacc**NNN**tttaagccgttcc-3'
Ala366for	5'-ggaacggcttaaa**NNN**ggtattaccgacgg-3'

Figure S1. *C. freundii* MGL dimer (*a*) and monomer (*b*), colored according to Consurf analysis. The most variable positions are colored turquoise, intermediately conserved positions are colored white and the most conserved positions are colored maroon. PLP is in yellow. The glittered shadow evidences one monomer with respect to the other in the dimer.

(*a*)

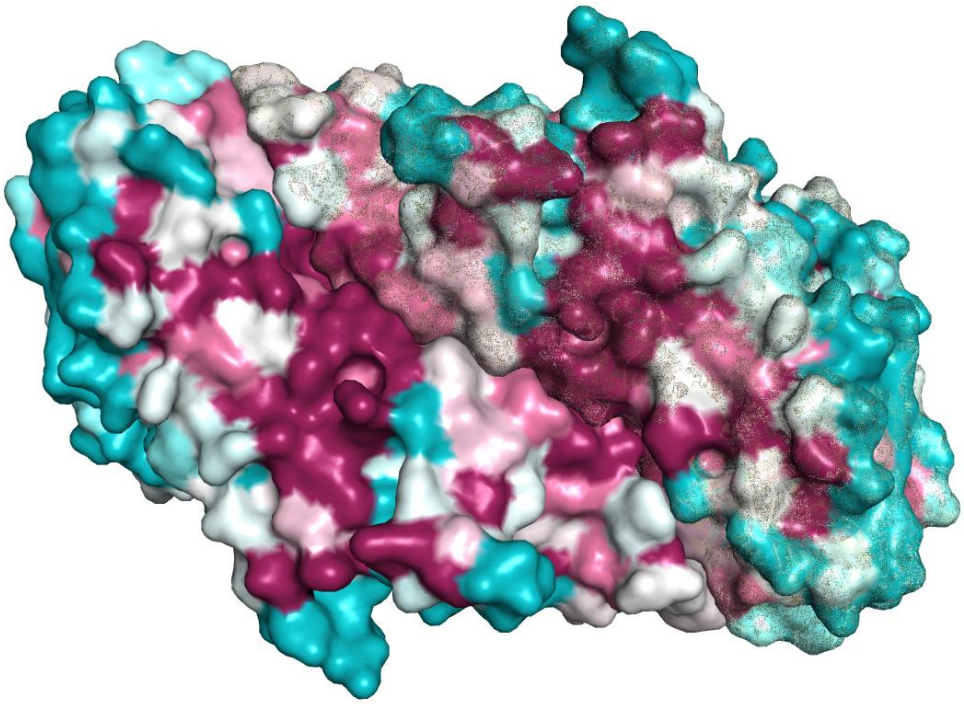

(*b*)

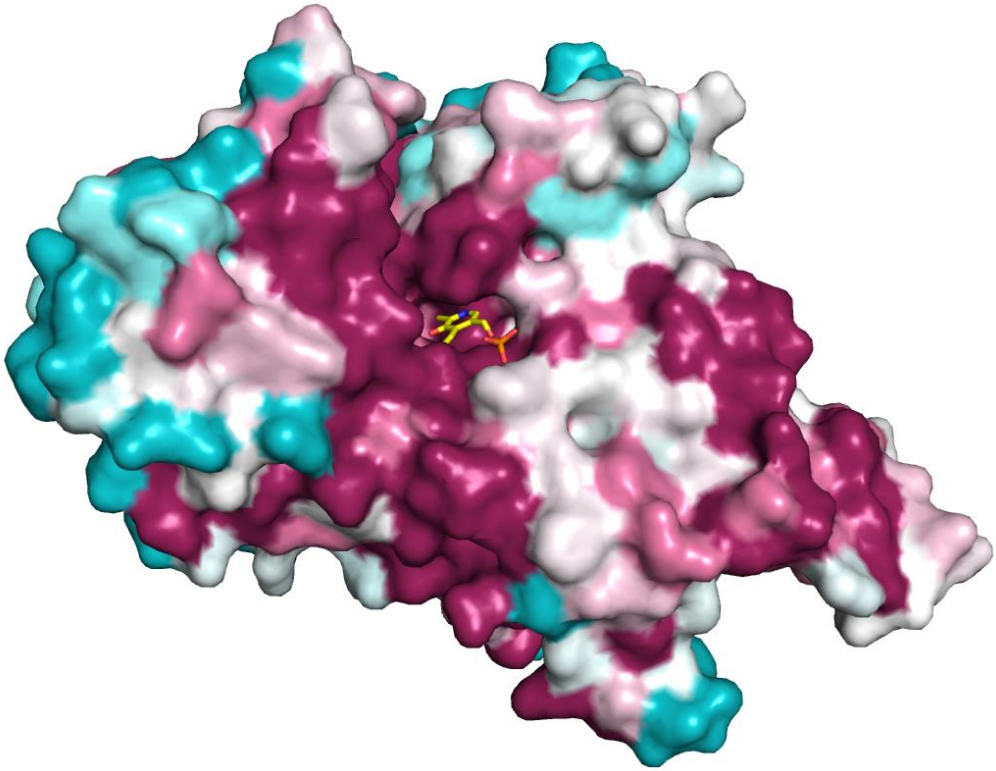

Figure S2. Specific activity of the ten purified variants generated by site-saturation mutagenesis for the α,γ-elimination reaction of L-methionine in the coupled assay with HO-Hxo-DH.

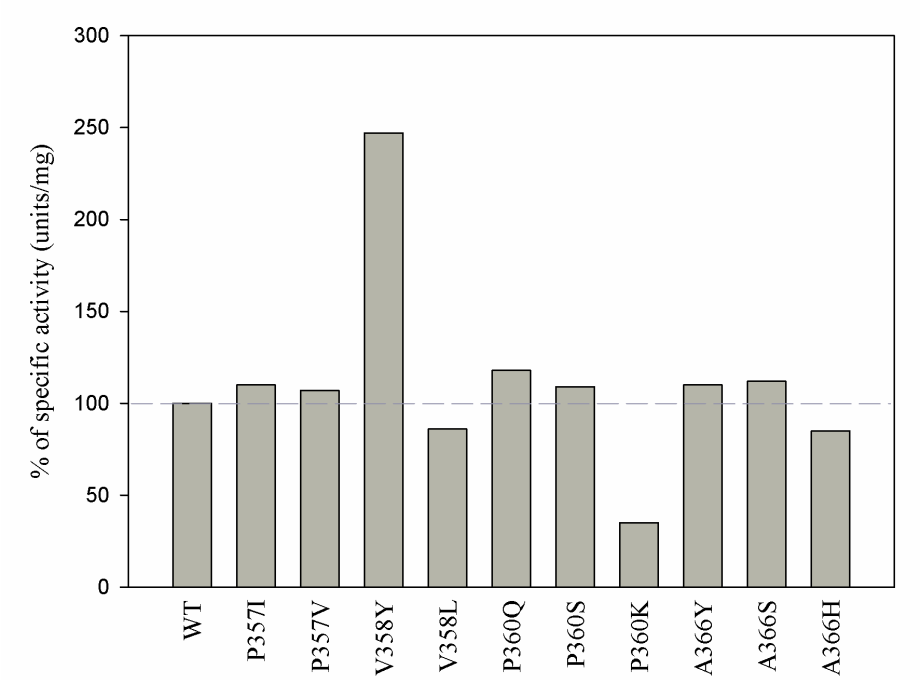

Figure S3. (*a*) Tetramer assembly of V358Y MGL. C-terminal mobile regions are shown in yellow. Y358 is shown in red with stick representation. PLP-binding sites are shown as red balls. (*b*) Superposition of the C^{α} traces of *C. freundii* MGL (PDB codes 1Y4I, 2RFV, 4P7Y, 5E4Z, 5M3Z, 5D5S, 6EGR, 3JW9, 3JWA, 3JWB, 4HF8, 4OMA, 3MKJ, 4MKJ, 4MKK, 5K30). The flexible regions are marked with red ovals. (*c*) Close-up view of the C-terminal mobile regions. Wild type holoenzyme MGL (PDB code 2RFV) is in blue, V358Y MGL (PDB code 6EGR) is in red, S339A MGL (PDB code 5D5S) is in yellow.

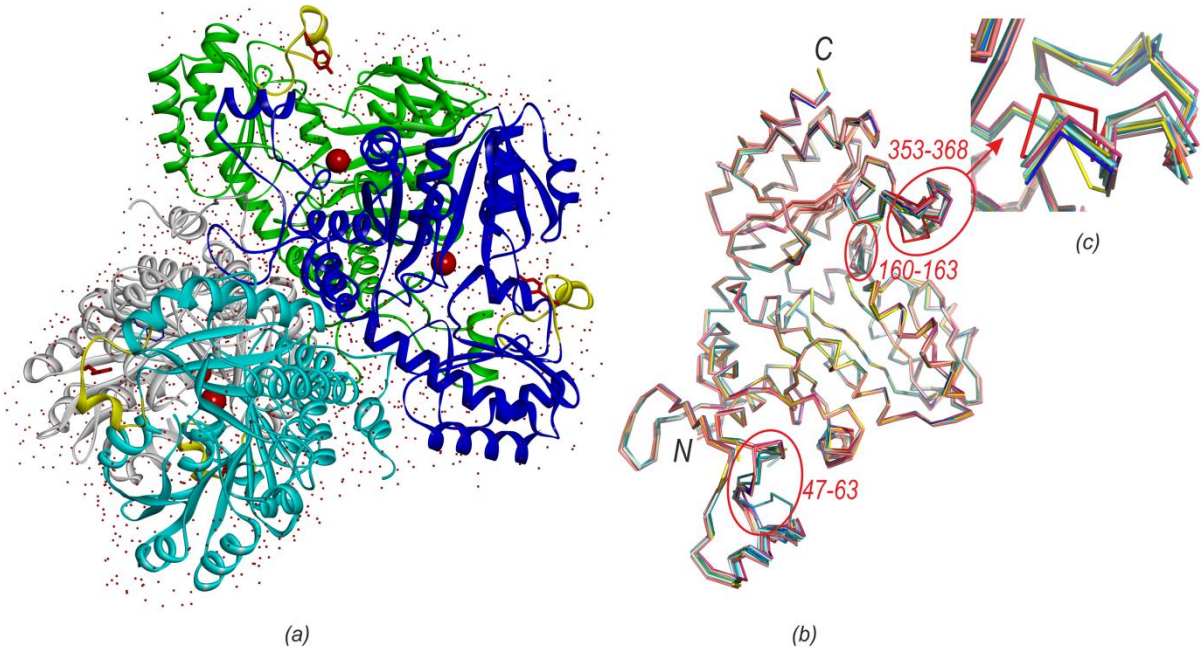

Figure S4. Stereo view of the superposition of active site residues of *C. freundii* MGL. V358Y MGL (black), wild type holoenzyme 2RFV (cyan) and wild type holoenzyme in complex with norleucine 3JWB (magenta). Residues from neighboring subunits are marked with asterisks.

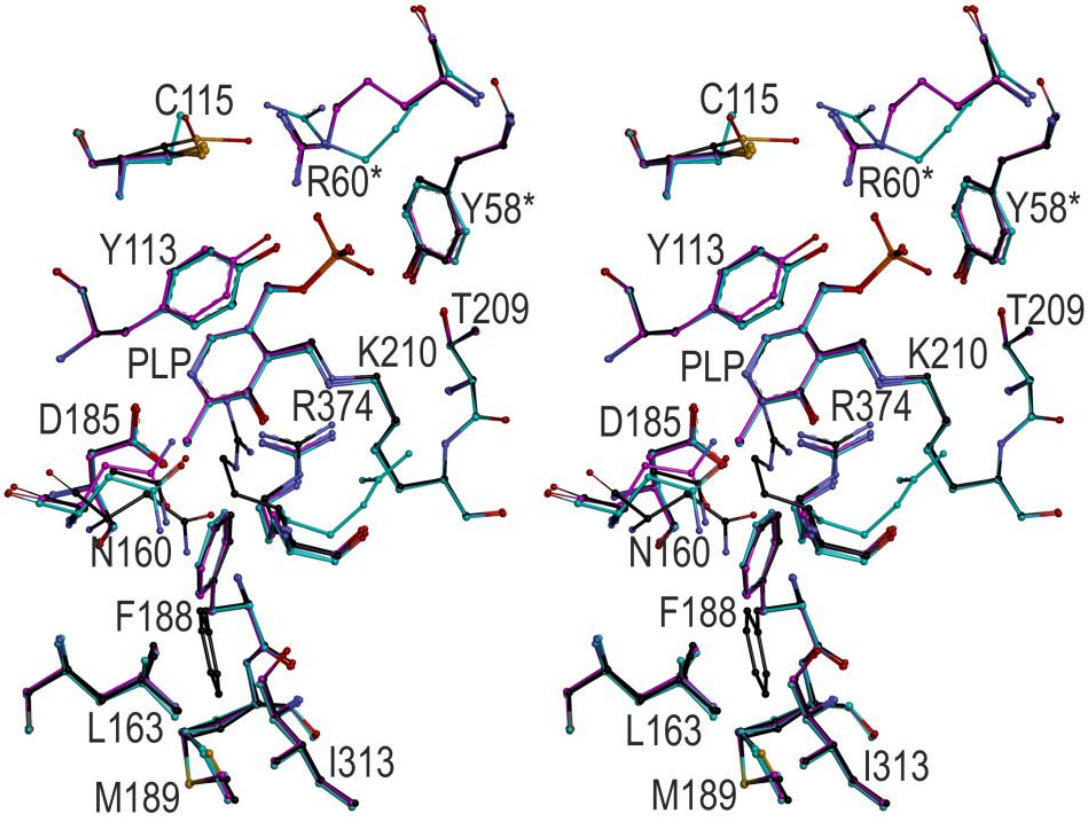

Figure S5. Alignment of the amino acid sequences of the C-terminal mobile region of MGLs from *Citrobacter freundii* (UniProtKB AC: Q84AR1), *Clostridium sporogenes* (UniProtKB AC: J7TA22), *Entamoeba histolytica* (UniProtKB AC: Q86D28), *Micromonospora echinospora* (UniProtKB AC: Q8KNG3), *Pseudomonas putida* (UniProtKB AC: P13254), *Trichomonas vaginalis*[1] (UniProtKB AC: O15564), *Trichomonas vaginalis*[2] (UniProtKB AC: O15565), *Arabidopsis thaliana* (UniProtKB AC: Q9SGU9), *Brevibacterium linens* (UniProtKB AC: Q5MQ31), *Clostridium novyi* (UniProtKB AC: A0A0Y0DCC0), *Clostridium tetani* (UniProtKB AC: Q890V5), *Fusobacterium nucleatum* (UniProtKB AC: Q8RDT4), *Porphyromonas gingivalis* (UniProtKB AC: F5XBR2), *Treponema denticola* (UniProtKB AC: Q73KL7).

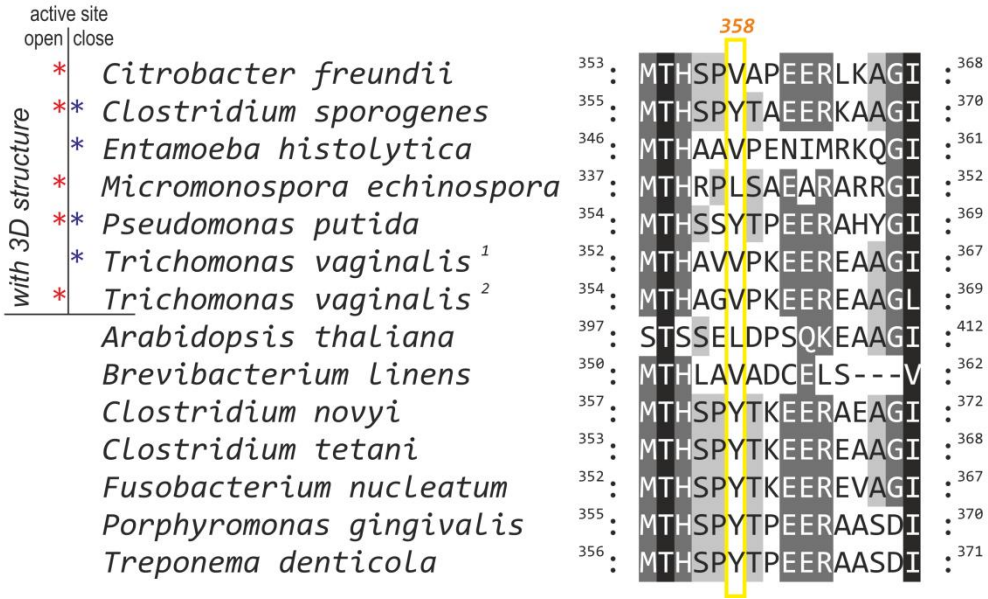

HIGHLIGHTS

- The C-terminal loop of *C. freundii* MGL is highly variant
- Most mutations at positions P357, V358, P360 and A366 cause enzyme inactivation
- Variant V358Y showed two-fold increase in catalytic rate and K_M.
- Comparison of X-ray structures of MGLs and V358Y suggests a conformational adaptation to mutations